University of Mohamed Kheider of Biskra
Exact Sciences and Sciences of Nature and Life
Matter Sciences

UNIVERSITY OF BISKRA

Final Dissertation in Master

Matter Sciences

Physics

Energy Physics and Renewable Energies

Presented by:

Cherroun Rima

Abdallaoui Doua

Study of n/p solar cell based on TCO/Si heterojunction

Jury:

Meftah Amjad	Professor	Med Khider University- Biskra	President
Meftah Afak	Professor	Med Khider University- Biskra	Supervisor
Laznek Samira	M.C. « B »	Med Khider University- Biskra	Examiner

Academic Year: **2019/2020**

بسم الله الرحمن الرحيم

السلام عليكم و رحمة الله و بركاته

" اللّهّم اِجعْلنا ممن
يتعلّمِ لِيَرقى ولا
تجعْلنا مِّمن يَتعلّم
لِيَشقى "
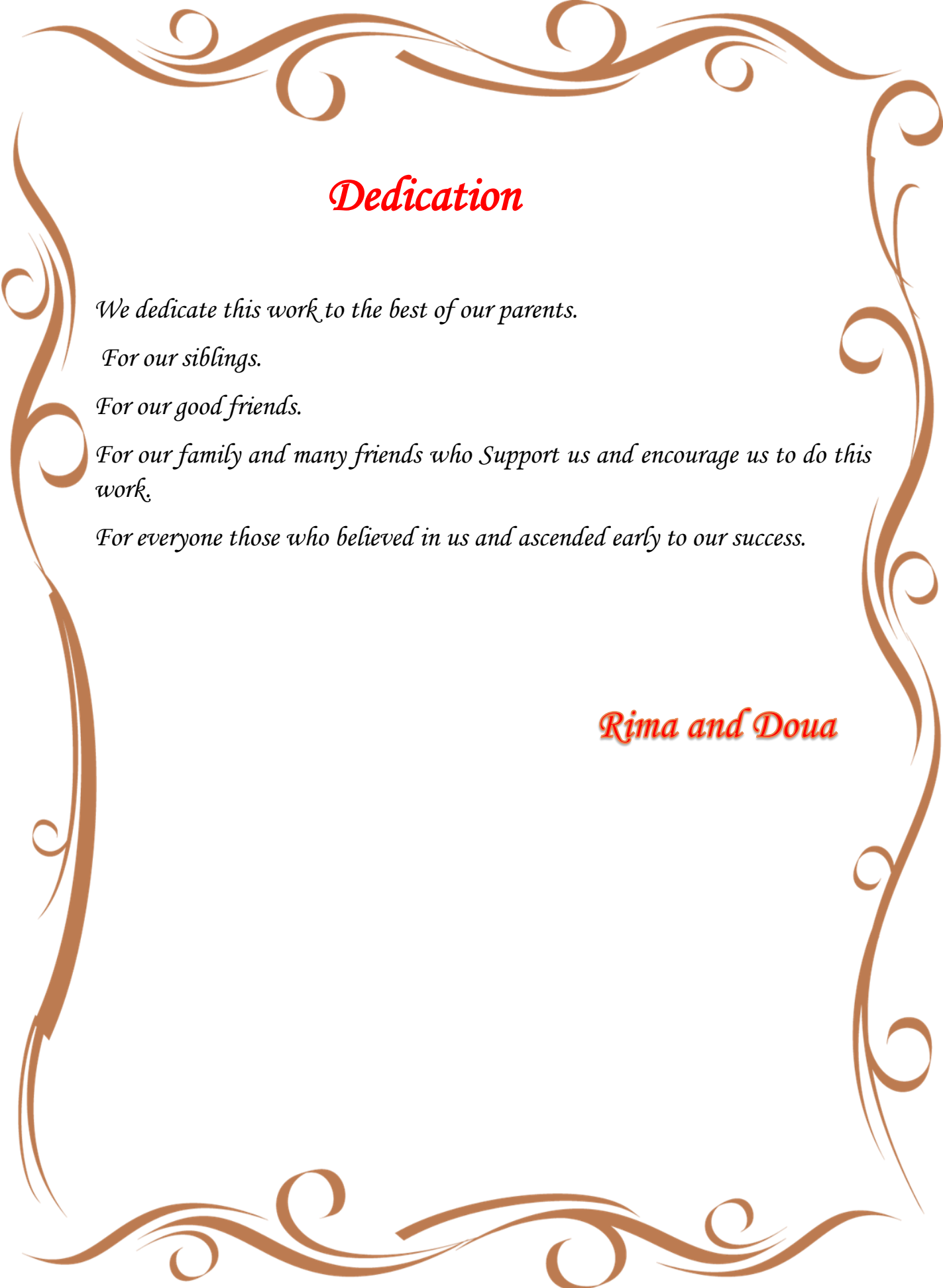
Dedication

We dedicate this work to the best of our parents.

For our siblings.

For our good friends.

For our family and many friends who Support us and encourage us to do this work.

For everyone those who believed in us and ascended early to our success.

Rima and Doua

Acknowledgements

We thank first and foremost to God; without his grace this thesis would never have been finished on time.

We would like to express our sincere gratitude to **Professor Counselors Meftah Afak** for the continuous support of our study and research that we conducted, for his patience, motivation, enthusiasm and tremendous knowledge. Help us direct it all the time researching and writing this letter. We never imagined a counselor and better mentor to study my masters.

In addition to our consultant, we would like to thank the rest of the doctoral thesis jury: **Professor Meftah Amjad** and the **Dr.Laznek Samira** for their comments and questions.

Of course, we do not forget the best friends we have had in our lives. Especially those who supported us in completing the beautiful memories, thank you, **Marwa**, **Khadija** and **Razika**. It was a short while but it meant a lot to us.

Last but not least, we would like to thank our family: **our parents**, **sisters**, and **brothers** for their spiritual support throughout our lives.

Rima and Doua

LIST OF TABLES

LIST OF FIGURES

LIST OF ACRONYMS

TCO   Transparent conductive oxides.

ZnO   Zinc oxide.

ITO   Indium oxide doped with tin.

TiO$_2$ Titanium dioxide.

Si   Silicon.

E_g Gap energy (eV).

$e\chi_s$ Affinity of the semiconductor (eV).

$e\phi_s$ Workfunction of the semiconductor (eV).

$e\phi_m$ Workfunction of the metal (eV).

ϕ_B The potential barrier of Schottky (eV).

E$_C$ Energy level of the conduction band.

E$_V$ Energy level of the valance band.

E$_F$ Fermi energy level semiconductor.

V_d Diffusion voltage (eV).

N_c Effective density of Conduction band (cm^{-3}).

N$_V$ Effective density of valence band (cm^{-3}).

D_n Diffusion constant of the electrons.

D_p Diffusion constant of the holes.

μ_n Electron mobility $(cm^2 V^{-1} s^{-1})$.

μ_p Hole mobility $(cm^2 V^{-1} s^{-1})$.

ε_r Relative dielectric constant.

B$_C$ Conduction band.

B$_V$ Valance band.

ρ The electrical resistivity $(\Omega.\,cm)$.

σ Electrical conductivity $(\Omega.\,cm)^{-1}$.

I_{sc} Short circuit current (A).

V_{oc} Open circuit voltage (V).

P_m Maximum power (w).

FF Fill factor.

η The Conversion efficiency.

Abstract

This work is a study by numerical simulation of an of heterojunction solar cells based on conductive oxide/Si heterojunction, the proposed cells are: ZnO(n)/Si(p), ITO(n)/Si(p), TiO$_2$(n)/Si(p) by Silvaco-Atlas software. Using host of improvements, we conclude that there is no big difference between the three studied cells. This does not prevent us from concluding that ZnO(n)/buffer/Si(p) solar cell provides best outputs of the solar cell with: $\eta = 22.30\%$; $J_{sc} = 39.81 mA / cm^2$; $FF = 0.838$; $V_{oc} = 0.668\, V$.

Key words: numerical simulation, Silvaco atlas, solar cell heterojunction, ZnO, ITO,TiO$_2$, J-V characteristic.

ملخص

هذا العمل عبارة عن محاكاة عددية لخلية شمسية غير متجانسة مكونة من أكسيد موصل/سليكون، الخلايا المقترحة هي:ZnO(n)/Si(p) ،ITO(n)/Si(p)، TiO$_2$(n)/Si(p) بواسطة برنامج المحاكاة سلفاكو–أطلس وباستخدام مجموعة من التحسينات نجد ان الخلية الشمسية ZnO(n)/buffer/Si(p) لديها أفضل وسائط الخروج المستخرجة من الخاصية جهد–تيار وهي:

$$\eta = 22.30\% ; J_{sc} = 39.81 mA / cm^2; FF = 0.838; V_{oc} = 0.668\, V.$$

ولكن عموما يوجد تقارب بين وسائط الخروج للخلايا الثلاث.

الكلمات المفتاحية

محاكاة عددية، سلفاكو–أطلس، خلية شمسية غير متجانسة، أكسيد الزنك، أكسيد الانديوم مطعم بالقصدير، أكسيد التيتانيوم، الخاصية تيار–جهد.

LABLE OF CONTENTS

References

Abstract

Introduction

Introduction

Transparent conductive oxides (TCO) are remarkable materials in many fields. The existence of their dual property, electrical conductivity and transparency in the visible, in addition to mechanical durability, including flexibility , makes them ideal candidates for applications in optoelectronics, photovoltaic or even as electro-chromic windows [1] .

With energy gap greater than 3.1 eV, most of these TCO materials have an insulating character. These properties depend not only on its chemical composition, but also and above all on the method used for its preparation. In addition to being transparent, they can become conductive (of type n for example :ZnO, In_2O_3, SnO_2…and type p :NiO,SnO, $CuCrO_2$…) if they have an excess of electrons and holes in their network, which can be created either by structural defects inducing an imbalance in the oxide geometry, or by appropriate doping [2] .

Traditional crystalline silicon (C-Si) solar cell structures make use of n-p junctions to separate photogenerated carriers by behaving as selective contacts due to the built in potential. However, they provide poor selectivity due to back injection over the barrier. In addition, the high temperature processing required for dopant diffusion during junction formation results in the degradation of the semiconductor bulk properties. It has been stated that significantly improved contact selectivity is necessary for achieving quantum efficiencies higher than 25% [3].

The use of TCO in heterojunction C-Si solar cells as transparent electrodes, and as n or p type layers in a solar cell is an economically viable photovoltaic technology [4]. They form efficient selective solar cell contact if they fulfill the requirements of high optical transparency, high surface passivation, and low series resistance. Among n type TCO are : tin doped Indium oxide (ITO), Zinc oxide (ZnO), and Titanium dioxide (TiO_2) which is the most used on an industrial large scale since it is non-toxic, good cost and abundance [5].

The work presented in this dissertation focused on the study and simulation of TCO(n-type)/Si(p-type) heterojunction solar cells. In the aim to confirm which n-TCO form the best electron selective contact, comparison is done between three suggested TCO(ITO,ZnO,TiO_2) that are used also as optical window in order to improve the photovoltaic performance and reduce the number of associated layers.

The dissertation is divided into three chapters as follows:

The first chapter is an overview on properties of n type conductive oxides for Si solar cells where the electrical, optical and structural characteristics of each material are presented (Oxides ITO, ZnO, TiO_2) silicon).

The second chapter presents basic notions relating to the heterojunction solar cell: definition, types, its operating principle, and examples of J-V characteristics of n-conductive oxide ITO, ZnO, TiO_2) /p -Si solar cells.

The third chapter is divided into two parts: the first part is consecrated to the simulation process performed by Silvaco-Atlas software. In the second part, we present the results of the simulation study of three solar cells ITO/Si, ZnO/Si and TiO_2/Si to compare between them and conclude which of these three TCO is the more suitable. In addition, the effect of several parameters is presented: thicknesses, doping, contact work function and the properties of the interface layer TCO/Si. Analysis and interpretation of these simulation results allow us to draw conclusion concerning the optimal parameters leading to the best performance of TCO(n)/Si(p) solar cells.

Chapter I:

Overview on n type conductive oxides for Si solar cells
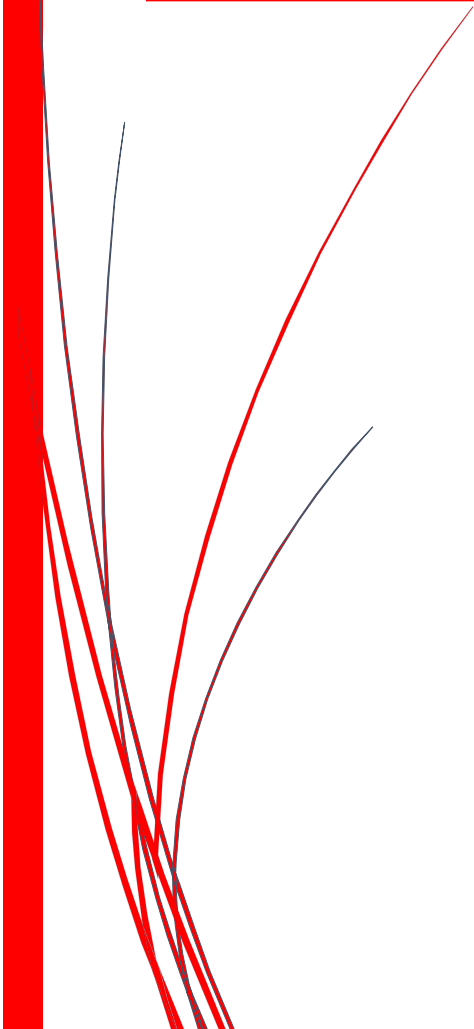
I.1.Introduction

Transparent conductive oxides TCO characterized by their high electrical conductivity and optical transmission properties in the visible spectral range. The famous and used TCO_S are degenerate oxides of n type consisting of metal oxides such as indium oxide (In_2O_3), zinc oxide (ZnO), tin dioxide (SnO_2), and their derivatives for example: Indium oxide doped with tin (In_2O_3: Sn or ITO), zinc oxide doped with aluminum (ZnO: AL) or tin oxide doped with fluorine (SnO_2: F or FTO) [1].

I.2.Properties of Zinc oxide (ZnO)

Zinc oxide is an inorganic compound with the formula ZnO. ZnO is a white powder that is insoluble in water, and it is widely used as an additive in numerous materials and products including rubbers, plastics, ceramics, glass, cement, lubricants, paints, ointments, adhesives, sealants, pigments, foods (source of Znnutrient), batteries, ferrites, fire retardants, and first aid tapes. It occurs naturally as the mineral zincite, but most zinc oxide is produced synthetically [2].The choice of zinc oxide comes from the reasons previously mentioned its several physical properties and variant applications in different domains. It has distinct advantages over other competitors, abundance in earth crust, non-toxicity, low material costs, chemical stability, high transparency in the visible and near infrared spectral region, etc. [2].

I.2.1.Structural properties of ZnO

ZnO belongs to the group of II-VI binary compound semiconductors which crystallize in either a cubic zinc blende or hexagonal wurtzite structure where each anion is surrounded by four cations at the corners of a tetrahedron, and vice versa. These materials also have substantial ionic character. Therefore, as shown in Figure.I.1, so there are three different types crystal structures of ZnO [5]:

❖   The hexagonal structure stable under normal conditions.
❖   The cubic structure which is unstable and which appears under high pressures.
❖   The Rock Salt structure.
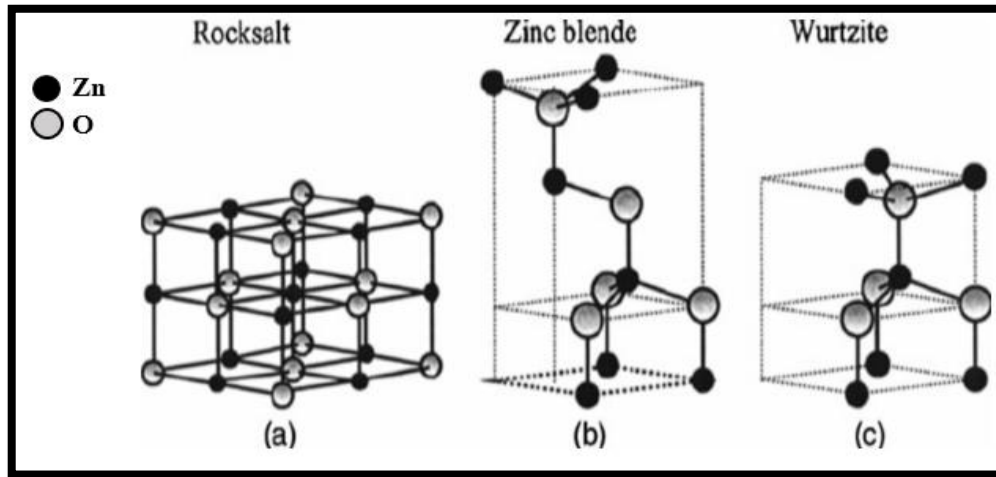
Figure.I.1: ZnO crystal structures: (a) cubic rock salt, (b) cubic zinc blend and (c) hexagonal wurtzite [2].

I.2.2.Electrical properties of ZnO

ZnO is a semiconductor with direct wide band gap energy, $E_g = 3.4 \, eV$ in ambient temperature [5]. It has piezoelectric properties due to its axial symmetry and high electrical conductivity $\boldsymbol{\sigma}$ ($> 5 \times 10^3 (\Omega.cm)^{-1}$)as n-type semiconductor [5].

The electrical resistivity $\boldsymbol{\rho}$ of ZnO films is determined by the carrier concentration **n** and carrier mobility $\boldsymbol{\mu}$ as follows:

$$\rho = \frac{1}{n \cdot e \cdot \mu} \tag{I.1}$$

Where **e** is the electron charge .To obtaining low resistivity, n and μ should be both maximal, and most research papers have suggested that the method to achieving this is by doping or introducing oxygen vacancies [2].

I.1.3.Optical properties of ZnO

ZnO is transparent in the visible range suitable for solar cells. for thin layers, we can distinguish three zones for $AM_{1.5}$ spectrum according to the transmission spectrum [2], shown in Figure.I.2:

❖ A total absorption in the ultraviolet range that corresponds to photons with high energy exceeding the band gap energy of ZnO.

❖ A very high transmission (low absorption) in the visible range for photons with energy lower than the band gap energy.

❖ A low transmission (high reflection) in infrared range when the $AM_{1.5}$ spectrum decreases considerably.
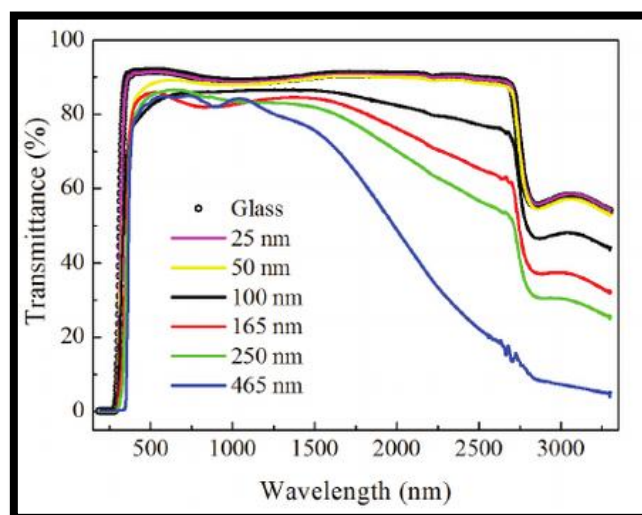
Figure.I.2: Optical transmission of (ZnO: AL) thin film for different thicknesses [6].

Some of the optical parameters of ZnO are given in Table.I.1 including transmittance, refractive index, maximal absorption and optical band gap energy.

Table.I.1: Some optical properties of ZnO[7].

Properties	Values
Transmittance in the visible.	$(80 - 90)\%$
Refractive index at 560 nm.	$(1.8 - 1.9)$
Absorption coefficient.	$10^4 cm^{-1}$
Optical gap.	$3.4\ eV$

I.3.Proprieties of Indium oxide doped with tin (ITO)

ITO is one of the most widely used transparent conductive oxides "TCO" in technological applications due to its remarkable optical and electrical properties: high transparency, good electrical conductivity, good mechanical resistance, excellent adhesion to substrate in addition to chemical stability. ITO is formed from indium oxide (In_2O_3) and a few atomic percentages in tin (Sn), generally 10%, which will replace the positions of the indium atoms

in the crystal and if the concentration of tin increases, electrical conductivity improves but transparency will be impaired [7-9].

I.3.1.Structural properties of ITO

The ITO has a structure very similar to that of indium oxide, In_2O_3 with the existence of oxygen vacancies. Depending on the production conditions, the ITO can be presented in two forms: the first is cubic and the second is hexagonal [10-12].

I.3.1.1.Cubic structure of ITO

Unique properties of ITO come from its structure and composition. Indium oxide has a cubic bixbyite structure which is shown in Figure.I.3. One unit cell contains 16 units of In_2O_3. Therefore, for defect free In_2O_3 crystal, there are 80 atoms in one unit cell. The lattice constant is reported to be 10.118Å [8]. The theoretical density is 7.12 $g\ cm^{-3}$ [12].
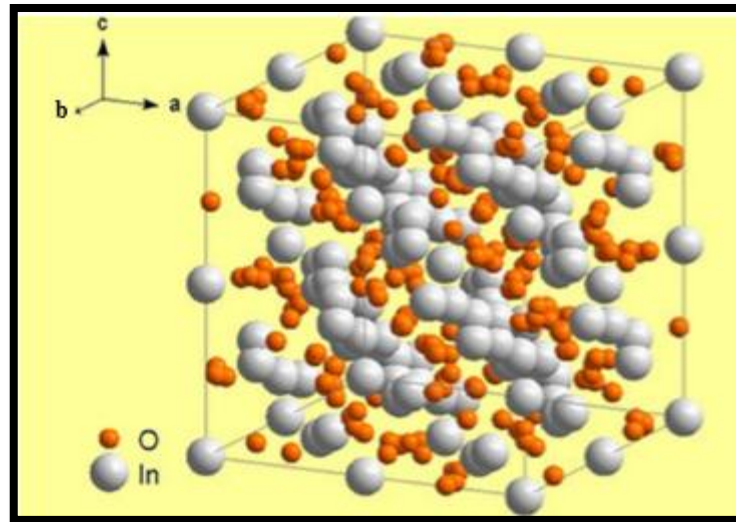
Figure.I.3: Elementary bixbyite of lattice In_2O_3.

Two kinds of non-equivalent indium sites are present in In_2O_3 crystal structures which are shown in Figure.I.4 [10]. In Figure.I.4(a), the separation between indium and oxygen atoms is 2.18 Å, and the oxygen atoms are positioned at the corners of the cube with two body-diagonally opposite corners unoccupied. In Figure.I.4(b), the (In-O) separations are 2.13, 2.19 and 2.23Å; where the oxygen atoms occupy positions at the corner of the cube with two face diagonally opposite corners unoccupied. Based on the description above, both indium sites can be viewed as an incomplete body centered cubic structure with an indium

atom located at the center and oxygen atoms at the corners. To change material properties, In_2O_3 can be extrinsically doped with tin. When tin atoms substitute for indium atoms, it forms either SnO or SnO_2. The material retains its bixbyite structure. However, if the doping level is extremely high, the tin atoms may enter interstitially and distort the lattice structure. As a polycrystalline structure, the ITO crystal grain size depends on various processing parameters such as substrate temperature and deposition rate [13,14].
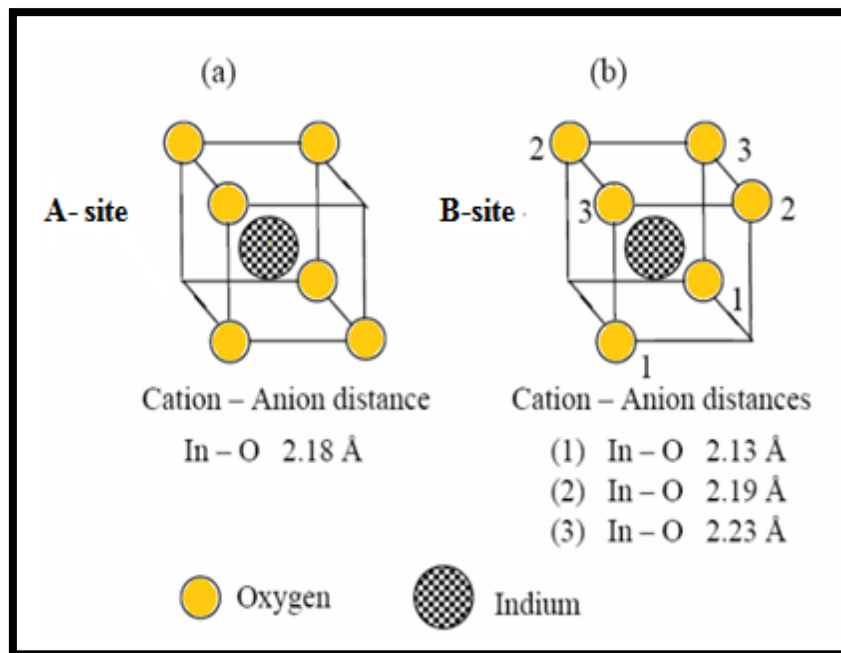
Figure.I.4: Two indium sites of ITO films [10].

I.3.1.2.Hexagonal structure of ITO

The ITO has another crystal structure of hexagonal type. This structure is obtained for exceptional working conditions of pressure and temperature (example 65kbar is $10^3 C°$) or in the case of a strong doping [10]. In this structure, the elementary lattice contains six lattices of indium oxide In_2O_3 where in this case, the parameters of lattice are equal to 5.49Å and 14.52Å, the density is 7.30 $g\ cm^{-3}$ [11].

I.3.2.Electrical properties of ITO

Indium oxide is a wide gap semiconductor. The band gap In_2O_3 was reported to be $3.75 eV$[15]. Generally, In_2O_3 crystal structure is not ideal since oxygen vacancies are present. Oxygen vacancies dominate the conduction mechanism of In_2O_3 and the free charge carrier concentration has been reported to be in the range $(10^{19} - 10^{21})cm^{-3}$. Extrinsic doping can vary the electrical properties of indium oxide significantly. If $In_2O_3$is doped with tin atom, tin atoms will replace indium atoms and form tin oxide in either SnO or SnO_2 depending on the valence. If SnO is formed, tin acts as an acceptor since it accepts an electron. Otherwise, when SnO_2 is formed, it acts as donor since it gives off an electron. Usually, SnO_2 dominates, and tin atoms act as donors. both tin and oxygen vacancies contribute to the conductivity of ITO [16].

The doping level is critical for electrical properties. As the tin concentration increases, the carrier concentration increases until a saturation level is reached. An increase in the tin concentration above this saturation level causes a decrease in the free carrier concentration. This is due to an increased probability of the occupation of adjacent cation positions by two or more tin atoms, which can deplete the active tin concentration. The carrier concentration as a function of tin doping level is illustrated in Figure.I.5. The highest carrier concentration, which corresponds to the lowest resistivity, occurs when the tin doping level is about 10%. The solid solubility of tin in indium oxide is approximately 8%. Beyond this range, tin oxide phase will be formed and distort the lattice structure. This will eventually cause a decrease of free carrier concentration [16].
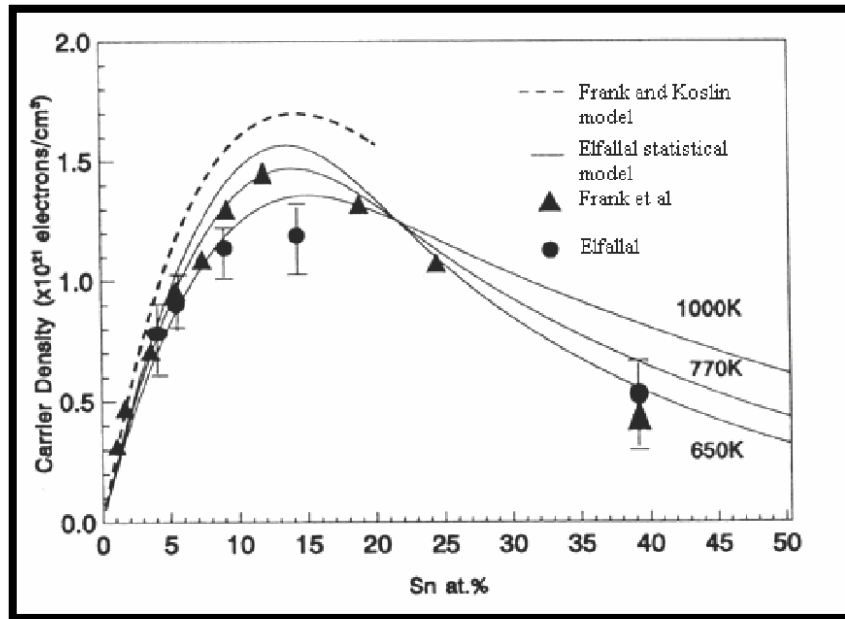
Figure.I.5: Carrier concentration as function of the tin doping level [16].

In order to get conductivity $> 10^3 (\Omega \, cm)^{-1}$ and avoid the formation of tin oxide phase, the doping level is typically chosen to be (8-10) %. This doping level will produce degenerative ITO [13]. Figure.I.6 shows the energy diagram of In_2O_3 and ITO , ITO has metal like electrical properties because the carrier concentration is typically around $(10^{19} - 10^{21}) cm^{-3}$, for heavily doped indium oxide, the contribution of oxygen vacancies to the conductivity is negligible [11].
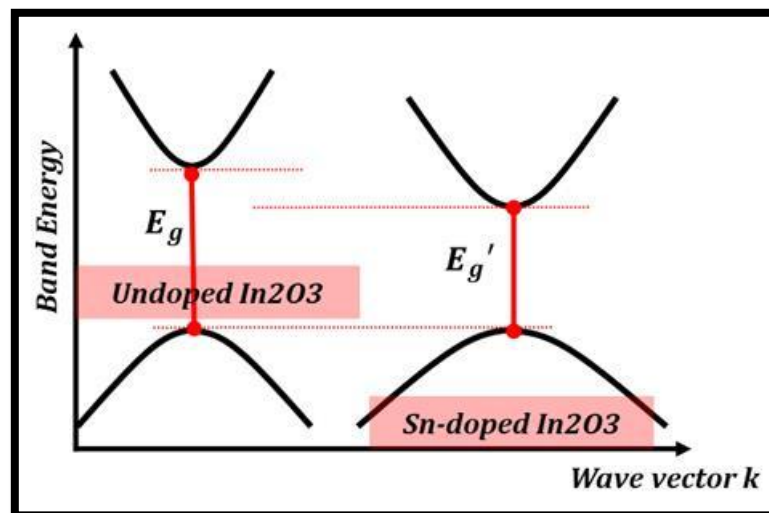
Figure.I.6: Energy diagram of In_2O_3 and ITO [11].

I.3.3.Optical properties of ITO

The ITO is characterized by a wide forbidden, direct band, which varies between $(3.5 - 4.3)\,eV$ [11], having a high absorption in the ultraviolet field, a good transmission in the visible, generally greater than 85%, and significant reflection in the infrared domain [17].
The value of the ITO refractive index is between 1.66 and 2.48 .The transmission of the ITO film is influenced by some factors such as the microstructure, the roughness and the homogeneity of the surface [18].

I.4. Properties of Titanium dioxide (TiO₂)

Titanium is the 9th most abundant element on earth (0.44% to 0.60% of the earth's crust according to estimates), discovered for the first time in the element ($FeTiO_3$). Titanium is a metal reduced simple body, its usual oxide is titanium dioxide chemical formula TiO_2, belonging to the family of transition metal oxides. It is a refractory product with a melting temperature of 1892 c° in oxygen and 1843 c° in air. TiO_2 is odorless, non-combustible, non-toxic that is obtained at low cost [16-19] .Titanium dioxide TiO_2 exists in three main allotropic forms: Rutile, Anatase, Brookite [16].

I.4.1.Structural properties of TiO₂

The elementary lattice motif is a more or less deformed octahedron (TiO_6). This motif consists of a titanium atom occupying the octahedral site surrounded by six oxygen atoms located at the summits of the octahedron as presented in Figure.I.7. The great distance (O-Ti-O) of the crystal lattice pattern merges with the direction [001] of the anatase and the direction [101] of the rutile [16].
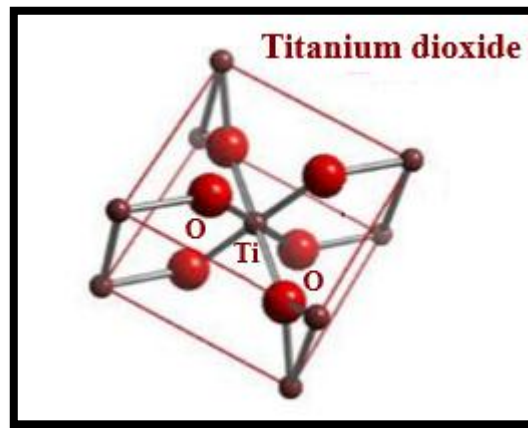
Figure.I.7: Unit cell of TiO_2.

I.4.1.1. Rutile TiO_2

The elementary lattice of rutile is quadratic (Figure.I.8), the bravais network is tetragonal and crystalline parameters are: a = b = 0.45933 nm and c = 0.29592 nm. It is the densest form of titanium dioxide, stable at high temperatures and high pressures, rutile TiO_2 is semi-insulating .Each titanium atom is surrounded by six oxygen atoms along an TiO_6 octahedron [20].
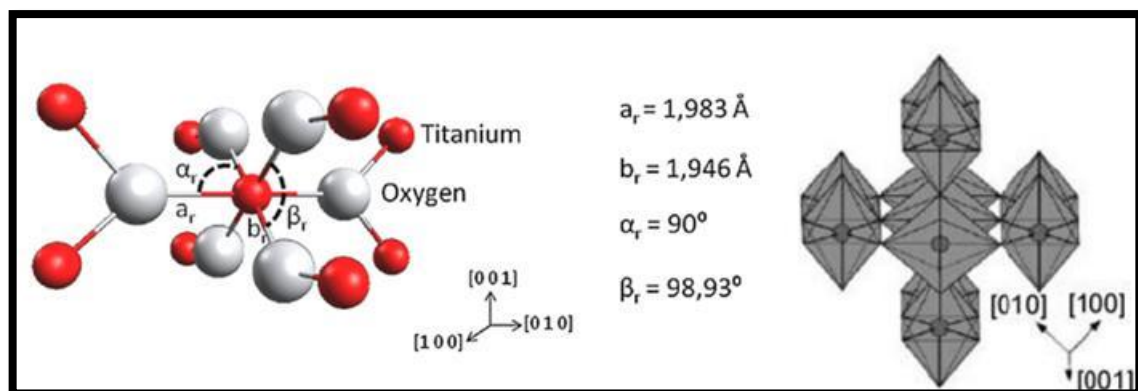
Figure.I.8: The structure of rutile TiO_2.

I.4.1.2. Anatase TiO$_2$

The elementary lattice of anatase is quadratic (Figure.I.9), bravais network is tetragonal and crystalline parameters are: a = b = 0.3785 nm and c = 0.9514 nm. TiO$_2$ anatase is a metastable phase which tends to evolve towards the more compact structure of rutile [20].

This structure is generally formed at lower temperatures than those of rutile formation and even more so of brookite. as a solid material, anatase is irreversibly transformed into rutile at a temperature of around 820 C° [21].
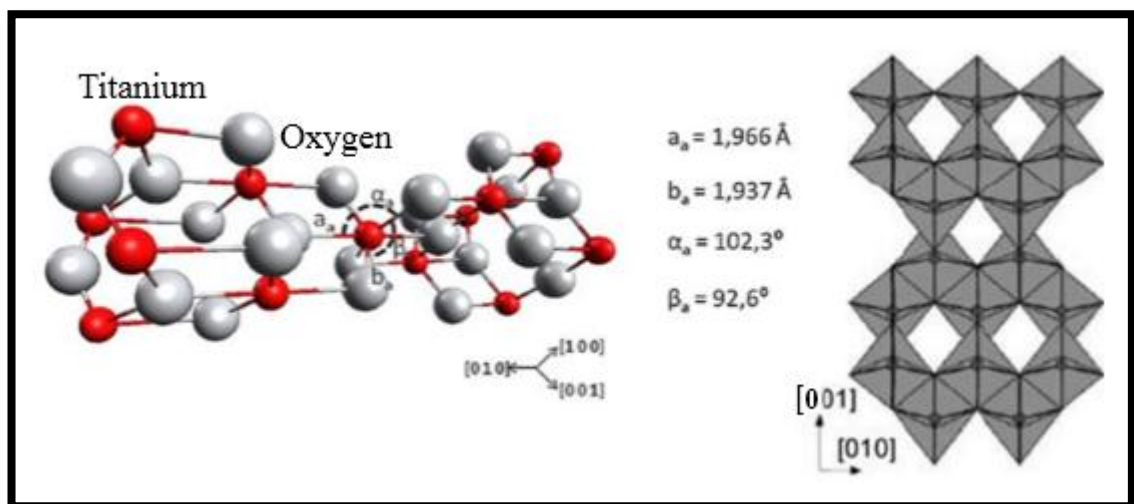
Figure.I.9: The structure of anatase TiO$_2$.

I.4.1.3. Brookite TiO$_2$

The structure of brookite (Figure.I.10), another metastable form of TiO$_2$, intermediate between anatase and rutile, brookite belongs to the orthorhombic crystal system and crystalline parameters are: a = 0.546 nm; b = 0.918 nm and c = 0.514 nm. It forms at low temperatures and at high temperature from 750C° the brookite transforms into rutile [21].
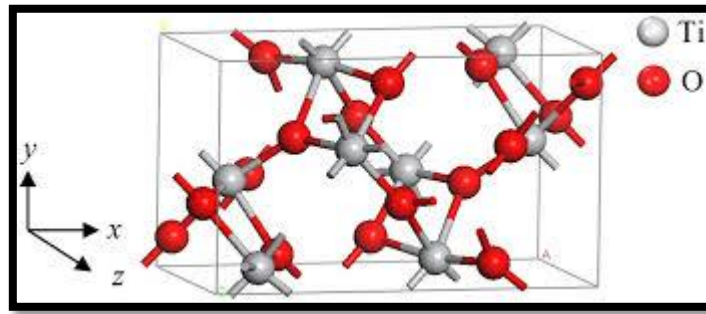
Figure.I.10: The structure of brookiteTiO$_2$

I.4.2.Electrical properties of TiO$_2$

The electronic band structure differs from one phase to another for titanium dioxide, because the width of the band prohibited at room temperature is 3.2 eV (380 nm) for the anatase, while in rutile form the forbidden band is 3 eV (407 nm) and finally in brookite form it is 3.14 eV (395 nm) [21] .

1.4.3. Optical properties of TiO$_2$

The optical transmission spectra of the TiO$_2$ films annealed at different temperatures are shown in Figure.I.11, which shows that all of the films were highly transparent in the visible region [22].
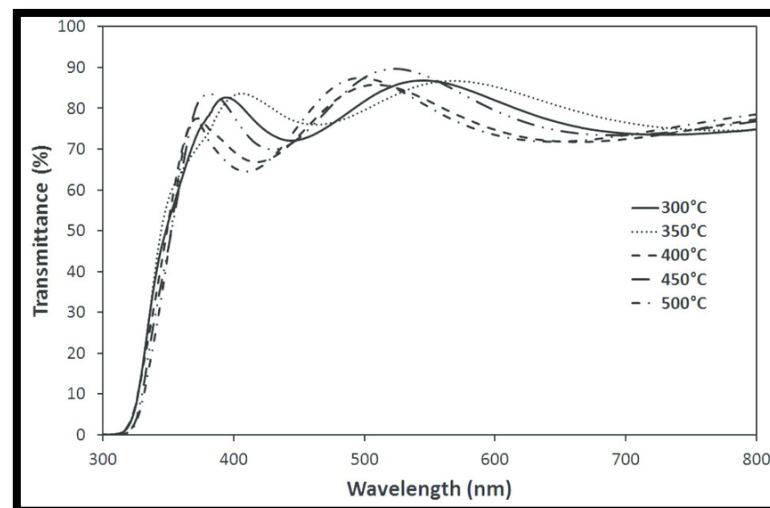
Figure.I.11: Transmittance of TiO$_2$ [22].

Table.I.2: transmittance value of the three forms of TiO_2 [23].

Transmission in the visible T (%) at 550nm.	Rutile	Anatase	Brookite
	92	90	90

I.5.Properties of silicon (Si)

Silicon is one of the main elements of clay, soils and rocks, under shape of semi-precious stones (Figure.I.12(a)).28.2% of the crust of our planet is made up of this mineral [24]. In fact, Si is almost as abundant as oxygen. Si is one of the essential elements in electronics, supported by the fact that current technology makes it possible to obtain pure Si at more than 99.99999% (Czochralski, floating molten zone) (Figure.I.12(b)). In addition, it is now possible to manufacture perfect silicon monocrystals with a volume of the order of m^3 [24,25].

(a)

(b)

Figure.I.12: (a) The mineral of silica [24] . **(b)** Silicon ingots [24].

I.5.1.Structural properties of Si

The crystal lattice of Si is that of diamond (Figure.I.13). It crystallizes according to the diamond lattice consisting of the superposition of two cubic sub networks with centered faces offset by a quarter of the main diagonal, the silicon lattice parameter is 5.43 Å [26].
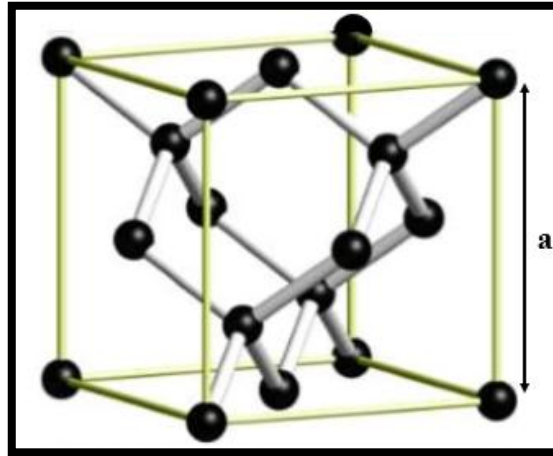
Figure.I.13: Unit cell of silicon.

I.5.2.Electrical properties of Si

The Si and the other elements of column IV of the periodic table (C, Ge) form covalent crystals. These elements generate covalent bonds, with their four neighboring atoms, by pooling their four valence electrons. The valence electrons in the case of diamonds have a high binding energy, which gives the diamond its insulating property (semiconductor with forbidden large band). This energy is zero in the case of tin, which makes it a good conductor. In the case of is this energy has an intermediate value at room temperature, making it a semiconductor allowing interesting applications. Si is a semiconductor which presents an energy band structure of the indirect type, which means that the maximum of the valence band (B_V) and the minimum of the conduction band (B_C) do not coincide in l space of the wave vector k. (Figure.I.14). during an electronic transition between the bottom of the (B_C) and the top of the (B_V) (recombination), or the opposite (absorption). There must be conservation of energy and momentum. In a direct forbidden band (GaAs) semiconductor, at the same value of k, the transition must only respect the energy conservation principle, so the energy of the emitted photon must be equal to Eg [27,28].
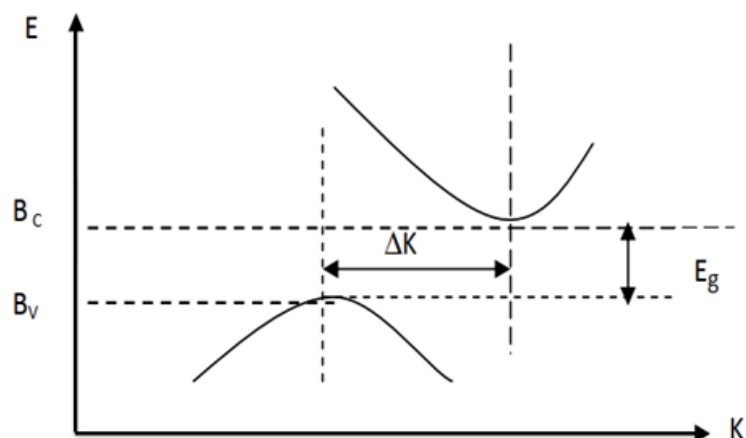
Figure.I.14: Energy band structure of crystalline silicon [27].

Table.I.3: Silicon electrical properties [27].

Properties	Values
Width of the energy band at 300 K.	1.12 eV
Electronic mobility at 300 K.	$\leq 1500\ cm^2.V/sec$
Thermal conductivity.	$1.5\ watt/cm^2\ C°$

1.5.3.Optical properties of Si

Table.I.4: Silicon optical properties [27-29].

Properties	Values
Refractive index in the visible.	$(4.925 - 3.57)$
Absorption coefficient in the visible.	$(10^5 - 10^3)\ cm^{-1}$
Optical gap in the visible.	1.12 eV
Reflectance.	35%

Chapter II:

n type conductive oxides for Si solar cells
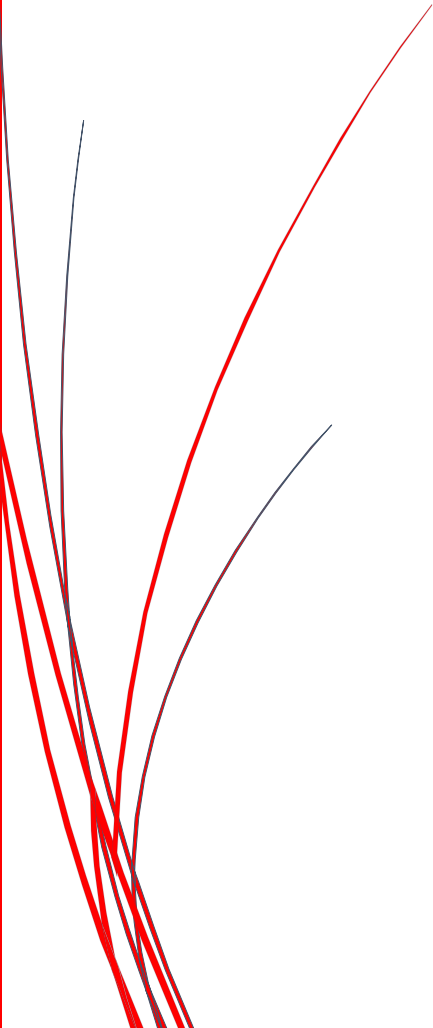
II.1.Introduction

The conversion of solar energy is the result of the absorption of photons giving rise to the creation of electron-hole pairs. a permanent electric field, within the structure, allows the rapid separation of these charge carriers to avoid the phenomena of recombination [30].

In conventional solar cells, this electric field necessary for separation charge carriers, is created by a n/p junction generally produced by diffusion of the phosphorus on the same monocrystalline silicon substrate. However, the implementation of such cells comes at a high cost. In addition, the high reflectivity of silicon in the visible 35% [30], requires other alternatives. Carrier selective contacts are one of the essential requirements for solar cells to operate closer to their thermodynamic limit of maximum efficiency. An ideal selective solar cell contact must fulfill the requirements of high optical transparency, high surface passivation, and low series resistance. Among these are the TCO (transparent conductive oxide) – Si heterojunctions. To date, several TCO-Si heterojunctions have been studied, such as ITO-Si [31] , SnO_2-Si [32] and ZnO-Si [33].

The most important factors causing a decrease in the efficiency of a silicon solar cell are non-absorbing photons that have less energy than the energy range (hν $< Eg$) , and photons in the field of short wavelengths that absorb near the illuminated surface. The effect of these factors can be minimized by using a tandem link structure or a heterojunction link structure [30].

In this chapter, we will first present heterojunction types, then shed light on operation principal of heterojunction n-TCO /p-Si solar cell and give (J-V) characteristics of some heterojunction solar cells that will be studied in this dissertation: ZnO/Si, ITO/Si and TiO_2/Si.

II.1.Heterojunction types

II.1.1.Semiconductor-Semiconductor

A heterojunction is obtained when two different semi-conductor materials are associated and requires the use of semi-conductors having similar crystal properties (the size of the atoms must in particular be fairly close with unequal band gaps) [31]. Depending on the type of doping used for semiconductors, two heterojunctions are distinguished in Figure.II.15(a,b)[33]:

- ✓ The first are the isotype heterojunctions, for which the two semiconductors are of the same type of doping.

✓ The second are the anisotype heterojunctions, for which the two semiconductors are doped differently.

(a)   (b)
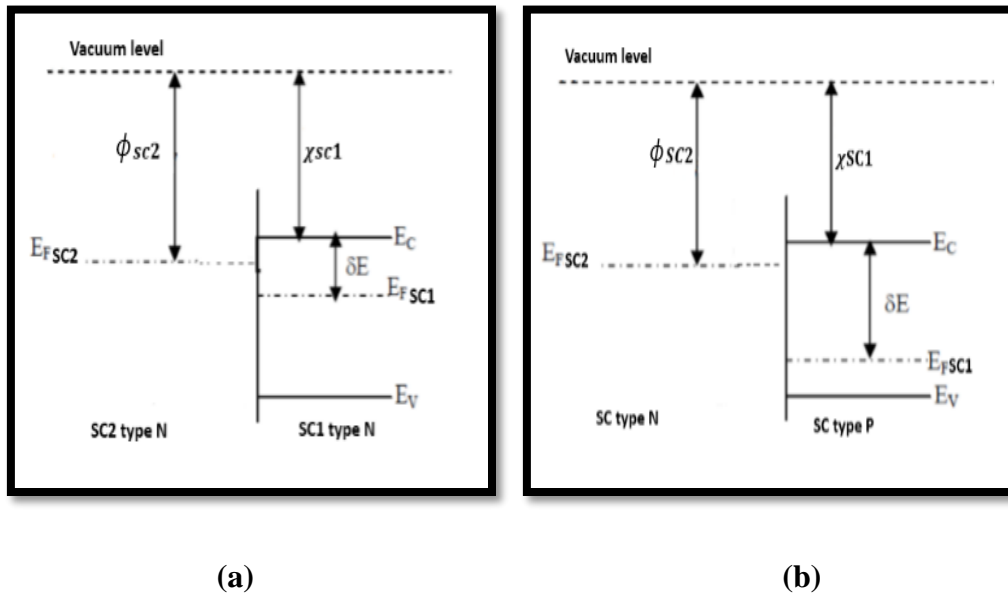
Figure.II.15: (a) Isotype heterojunctions [33].   **(b)** Anisotype heterojunctions [33].

Semiconductor interfaces can be organized into three types of heterojunction as shown in Figure.II.16 [33].
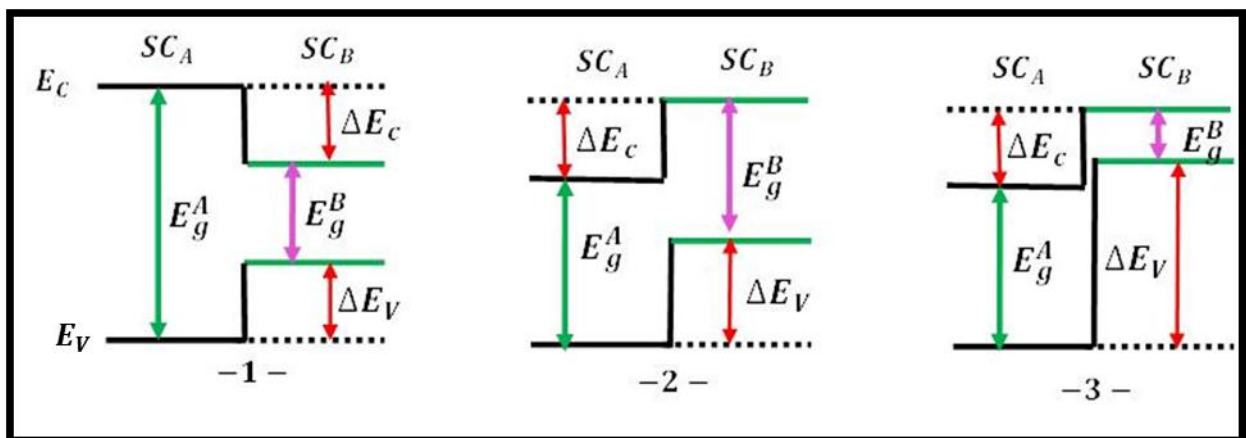
Figure.II.16: Schematic diagrams showing two different types of heterojunction [33].

• Type 1: The prohibited band E_g^B is entirely in E_g^A.

• Type 2: One of the discontinuities is greater than E_g^A - E_g^B but less than E_g^A.

• Type 3: One of the discontinuities is greater than E_g^A.

II.1.2.Metal-Semiconductor

Metal-semiconductor contact constitutes one of the basic devices of electronics modern. It is used both for its rectification properties (Schottky diodes) and to make good quality ohmic contacts [34].

When a metal and a semiconductor are in contact, an exchange of charges occurred so that the system finds a thermodynamic equilibrium. Band structure of energy at the interface of the metal-semiconductor contact is conditioned on the one hand by the type of the semiconductor and on the other hand of the possible difference between the metal work function $e\phi_m$ and that of the semiconductor $e\phi_s$ will then have the following cases [34]:

➢ When $e\phi_m > e\phi_S$: The semiconductor metal contact (n) is Schottky.

The semiconductor metal contact (p) is ohmic.

➢ When $e\phi_m < e\phi_s$: The semiconductor metal contact (n) is ohmic.

The semiconductor metal contact (p) is Schottky.

II.1.2.1.Ohmic contact

This contact is established when a carrier accumulation zone is published majority on the semiconductor side. The current-voltage characteristic must obey the law of ohm V = RI . The diagrams of the energy bands of such a contact are shown in Figure.II.17(a,b) [31]. We can see that the amplitude of the curvature of the bands and their extension in the semiconductor are very small. As a result, there is almost no barrier between metal and semiconductor. So electrons can circulate freely at through contact [34].

(a)   **(b)**
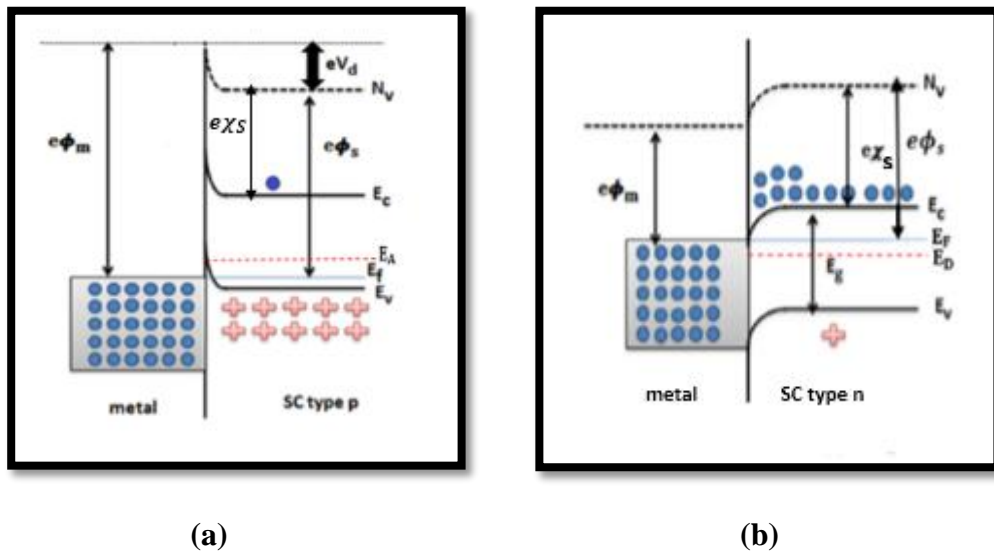
Figure.II.17: Metal-semiconductor ohmic contact in thermodynamic equilibrium **(a)** contact (p) with $\phi_m > \phi_s$ and **(b)** contact (n) with $\phi_m < \phi_s$ [34].

II.1.2.2.Schottky contact

This type of contact is obtained when an area deserted by majority carriers appears on the semiconductor side. When metal "M" comes into contact with a semiconductor, the levels are balanced Fermi is done by passing electrons from the metal to the semiconductor or vice versa, according to their work function as well as the doping of the semiconductor. This broadcast of electrons stops when the internal field generated by the space charge balances the diffusion current [34]. The energy diagrams of this type of contact are illustrated in Figure.II.18(a,b).

(a)   **(b)**
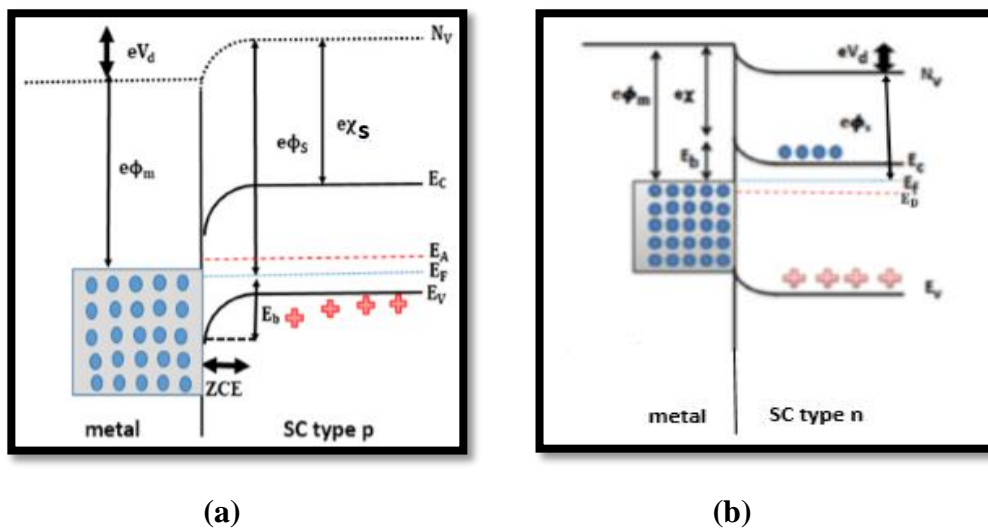
Figure.II.18: Metal-semiconductor Schottky contact in thermodynamic equilibrium **(a)** contact (p) with $\phi_m < \phi_s$ and **(b)** contact (n) with $\phi_m > \phi_s$ [34].

The potential barrier formed at the interface is called the Schottky ϕ_B, whose height is given by the difference between the metal work function and the electronic affinity of the semiconductor according to the following relationship [34]:

$$\phi_B = (\phi_m - \chi_S) \qquad\qquad\qquad\qquad (II.2)$$

ϕ_m : Metal work function.

χ_S : Electronic affinity of the semiconductor.

diffusion voltage V_d is given by [35]:

$$V_d = \phi_m - \phi_S = \phi_m - \chi_S - \frac{E_C - E_F}{q} \qquad\qquad (II.3)$$

E_C : Energy level of the conduction band.

E_F : Fermi energy level semiconductor.

II.2.Principal of n-conductive oxide / p-Si heterojunction solar cell

The TCO grown on Si can work as an active n-layer as well as anti-reflection (AR) coating due to its close refractive index match with the ideal value. This prevents requirement of additional anti-reflect coating which can reduce fabrication cost and complexity. Most of TCO can be deposited at much lower temperature that can reduce degradation in carrier lifetime, a common problem in high temperature diffusion of phosphorous and ion implantation in the conventional Si n/p junction solar cell [36].

The principal of n-TCO/p-Si differs slightly from that of n-Si/p-Si when light reaches the n-p junction, the light photons can easily enter in the junction, through thin n-type layer and Transparent as shown in Figure.II.19(a). The light energy, in the form of photons, supplies sufficient energy to the junction to create a number of electron-hole pairs. The incident light breaks the thermal equilibrium condition of the junction. The free electrons in the depletion region can quickly come to the n-type side of the junction. Similarly, the holes in the depletion can quickly come to the p-type side of the junction. Once, the newly created free electrons come to the n-type side, cannot further cross the junction because of barrier potential of the junction. Similarly, the newly created holes once come to the p-type side cannot further cross the junction became of same barrier potential of the junction. As the concentration of electrons becomes higher in one side, i.e. n-type side of the junction and concentration of holes becomes

more in another side, i.e. the p-type side of the junction, the n/p junction will behave like a small battery cell. A voltage is set up which is known as photo voltage. If we connect a small load across the junction, there will be a tiny current flowing through it. The available output voltage is related to the energy gap of the silicon, and depends on the doping levels and on the lateral voltage drops that exist in the thin top layer under current flow conditions. In heterojunction solar cells, it was shown that the output voltage is related to the energy gap of the base semiconductor that is the one with the smaller of the two energy gaps. The semiconductor with the larger energy gap acts primarily as a window to photons of energy less than its band gap. However the advantage of the heterojunction cell is that this window layer may be proportioned in thickness and doping to minimize the lateral resistance losses in the cell [37].

(a)   **(b)**
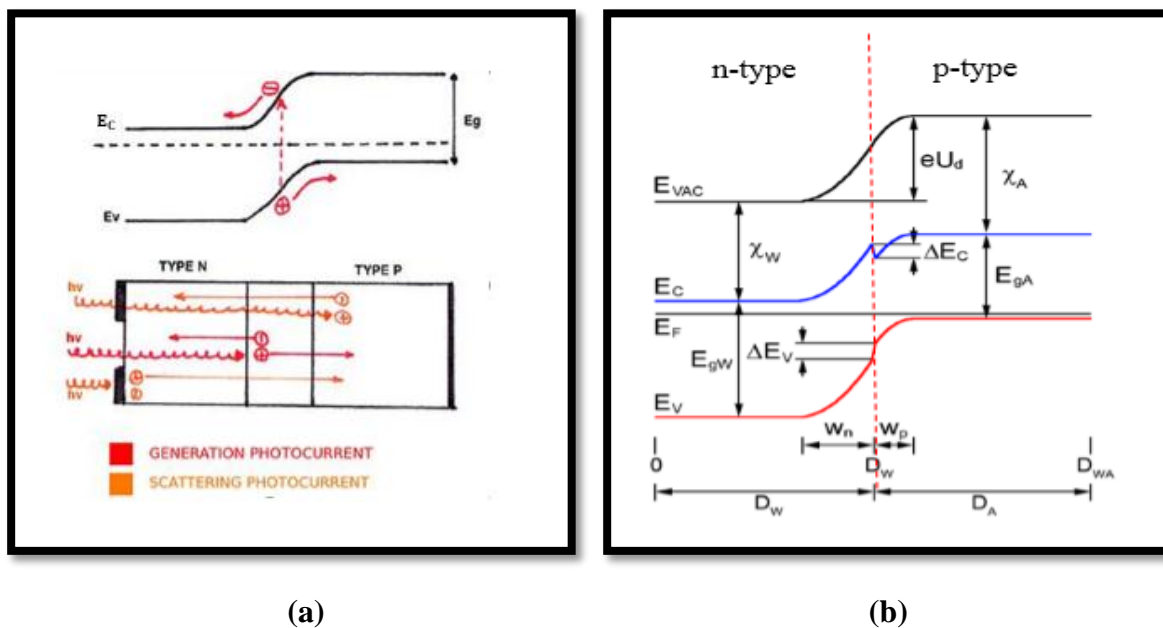
Figure.II.19: Principal of n /p solar cell: **(a)** homojunction **(b)** heterojunction.

In heterojunctions there is normally an energy spike ΔE_c, in the conduction band that is equal in principle to the electron affinity difference of the two semiconductors. There is also a valence band barrier step ΔE_V, which is $E_{gW} - E_{gA} - \Delta E_c$, as shown in Figure.II.19(b). For most heterojunction pairs, ΔE_c is considerably less than ΔE_V. Therefore there are advantages in selecting for consideration n-window/p-base heterojunctions. Then electrons flowing from the p base, where almost all the photon absorption takes place, are not seriously impeded by the

relatively small ΔE_c spike. In the other class of heterojunction, p large-gap/ n small gap, where the spike is ΔE_V, and is large, it is usual to observe a great deal of interface recombination.

A second reason for the n-window p-base choice is that most of the current is caused by electrons collected as minority carriers from the narrow band gap semi-conductor, and the diffusion length of electrons tends to be appreciably more than that of holes in the semiconductors of interest to us [37].

There are two types of currents, the first is related to minority carrier diffusion in neutral regions; n and p and known by diffusion current. The second one is due to the internal built in electric field at the n/p junction where the depletion region is formed, and named drift current.

The diffusion current of both electrons and holes is given by [38]:

$$\overrightarrow{J_{dn}} = +qD_n\overrightarrow{gradn} \tag{II.4}$$

$$\overrightarrow{J_{dp}} = -q\,D_P\overrightarrow{gradp} \tag{II.5}$$

D_n , D_p diffusion constant of electrons and holes respectively [38].

The drift current (traction current) of both electrons and holes is given by [38]:

$$\overrightarrow{J_{tn}} = qn\mu_n\vec{E} \tag{II.6}$$

$$\overrightarrow{J_{tp}} = qp\mu_p\vec{E} \tag{II.7}$$

$$\vec{E} = -\overrightarrow{gradV} \tag{II.8}$$

μ_n , μ_p mobility of electrons and holes respectively.

II.3. Example of J-V characteristics of some n-conductive oxide/p-Si solar cells

We present in this section some of experimental measurements of J-V characteristic for three types of n-type TCO/p-Si solar cells: ZnO/Si , ITO/Si and TiO$_2$/Si.
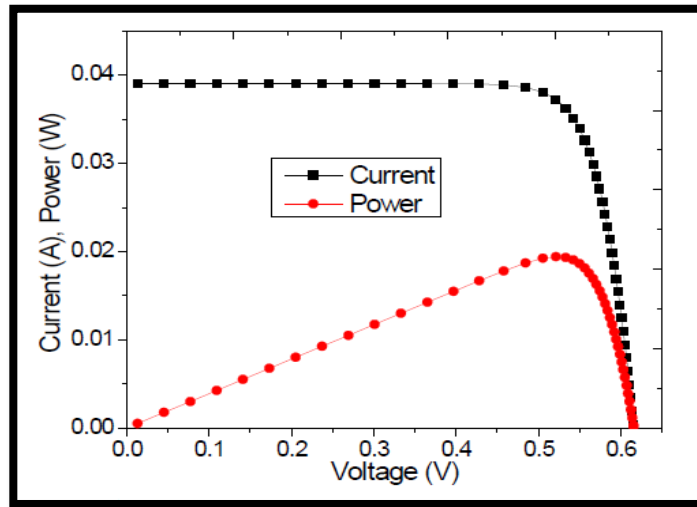
Figure.II.20: (I-V) and power characteristics of the ZnO/Si heterojunction solar cell in device area $1cm^2$ [39].
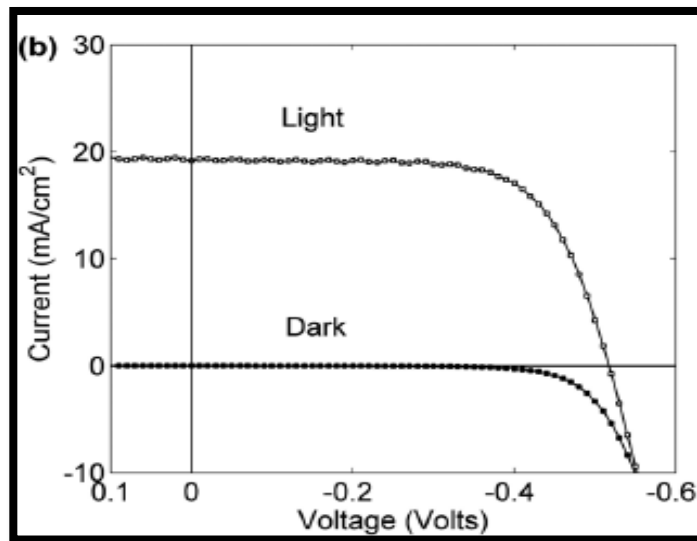
Figure.II.21: (J-V) curve of TiO$_2$/Si heterojunction solar cell in dark and in light [40].
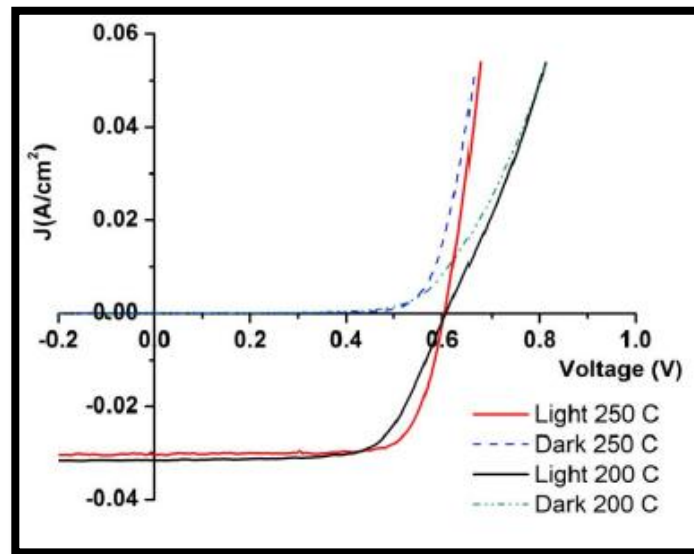
Figure.II.22: (J-V) curve of ITO/Si heterojunction solar cell [41].

II.4. Solar cell parameters

The principal parameters that characterize a solar cell are called photovoltaic parameters and are deduced from the current-voltage characteristic (J-V) mainly under illumination as shown in Figure.II.23.
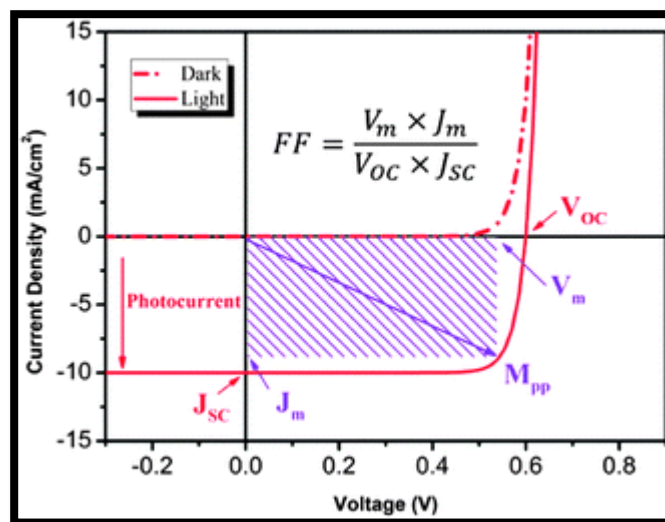
Figure.II.23: Current-voltage characteristic and physical parameters of a photovoltaic solar cells.

II.4.1.Short circuit current I_{SC}

The short circuit current I_{SC} (for V = 0) of the photovoltaic cell constitutes the maximum current, which can be obtained from a solar cell. In this case, the short circuit current can be considered to be equivalent to the photocurrent I_{ph} [42].

$$I_{SC} = - I_{ph} \tag{II.9}$$

II.4.2.Open circuit voltage V_{oc}

The open circuit voltage (V_{oc}) is the voltage for which the current across the cell terminals is zero (I = 0) [42]. The total current I_T is defined by the relation:

$$I_T = I_{ph} + I_d \tag{II.10}$$

$$I_T = I_{ph} - I_S[\exp(\frac{qV}{\eta K_B T}) - 1] \tag{II.11}$$

When $I_T = 0$, V= V_{oc} we find:

$$V_{oc} = \frac{\eta K_B T}{q} \ln\left[\left(\frac{I_{ph}}{I_S}\right) + 1\right] \tag{II.12}$$

Where:

I_{ph} : Photo-generated current by the solar generator under illumination(A).

I_d : The direct current of a solar cell(A).

V   : Voltage across the cell(V).

I_S : Saturation current of the solar cell(A).

K_B : Boltzmann constant and equal 1.38×10^{-23} J/K.

η : Ideal factor of the solar cell.

T   : Temperature(K).

q   : Electric charge(C).

II.4.3. Maximum power P_m

The output power of the cell (or generator) is the product of the output current delivered by the latter and the voltage across its terminals [43].

The value of the power at the short circuit point is zero since the voltage is zero. The power at the open circuit point is also zero since the current is zero. The power between these two points

is positive and the maximum power Point (PPM) of coordinates obtained for $V = V_m$ and $I = I_m$ such as [43,44].

$$P_m = V_m \times I_m \tag{II.13}$$

II.4.4. Fill factor FF

This is a rapport that reports on the quality of the shape of the I-V characteristic. It is defined by the following relation [43,44]:

$$FF = \frac{P_m}{V_{oc} \times I_{sc}} = \frac{V_m \times J_m}{V_{oc} \times J_{sc}} \tag{II.14}$$

The theoretical fill factor is between 0.25 and 1. In the case of an ideal cell, it cannot exceed 0.89 [43].

II.4.5.The Conversion efficiency η

It defines the relationship between the optimal electrical power obtained across the cell and the power of the incident radiation. It is given by [42]:

$$\eta_{photovoltaic} = \frac{P_m}{P_{int}} \times (100\%) = \frac{I_m V_m}{P_{int}} \times (100\%) = \frac{I_{sc} V_{oc}}{P_{int}} \times FF \times (100\%) \tag{II.15}$$

$$P_{int} = E \times S \tag{II.16}$$

E : Intensity of illumination in W/Cm^2.

S : The area of the solar cell.

II.5.Experimental photovoltaic parameters of the ITO/Si, TiO₂/Si and ZnO/Si

In the Table.II.5, we present examples of some experimental photovoltaic parameters of the ITO/Si, TiO₂/Si and ZnO/Si solar cells.

Table.II.5: Example of experimental photovoltaic parameters of n-TCO/p-Si heterojunction solar cells [45-47].

	$J_{sc}(mA/cm^2)$	$V_{oc}(mV)$	$FF(\%)$	$\eta(\%)$
ITO/Si	9.83	280	39.9	1.1
TiO$_2$/Si	2.93	301	31.8	0.28
ZnO/Si	25	375	72	6.79

Chapter III:

Numerical Simulation of a conductive oxide /Si heterojunction solar cell by **SILVACO-ATLAS**
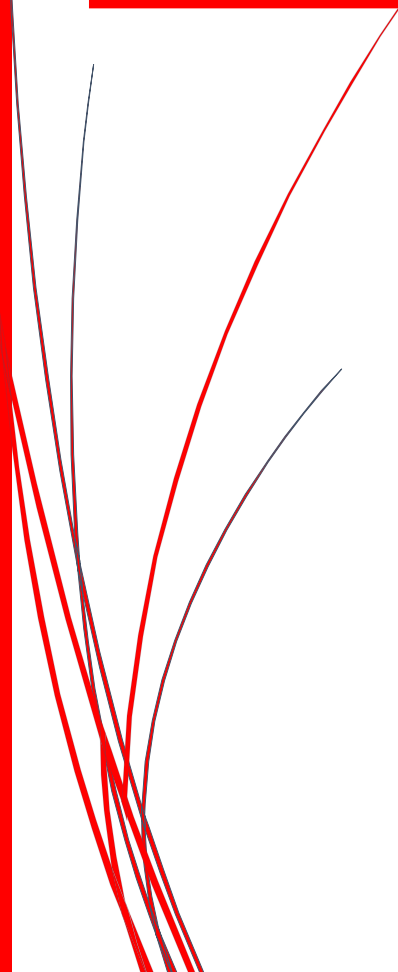
III.1.Introduction

The ATLAS device simulator, by Silvaco international, is a computer program which uses solid state physics and numerical analysis to simulate the behavior and characteristics of electrical devices [48]. In this chapter, the ATLAS simulator is used to study n/p solar cells based on conductive oxide /Si heterojunction. The studied cells are: ITO/Si, TiO$_2$/Si and ZnO/Si.

In the next sections, we will give the basic steps to work with ATLAS to simulate numerically the proposed cells and the extracted J-V characteristics, and the related electrical output parameters.

III.2.Physical model and simulation software

III.2.1.Device Structure

The solar cell structure is shown in the Figure.III.24. The front layer is a n-type transparent conductive oxide (TCO) and the second layer is a p-type crystalline silicon. The n-type layer constitutes anti-reflection coating and selective layer for electron while blocks holes. The chosen metallic contacts are silver (Ag) for the front contacts and gold (Au) for the back contact.
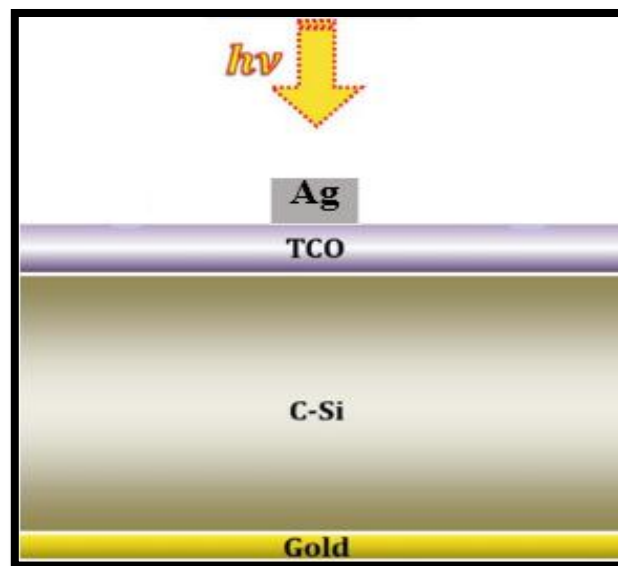
Figure.III.24: The structure of TCO(n)/Si(p) solar cell.

III.2.2. Principle of the SILVACO-ATLAS simulator

This device simulator is based on the simultaneous resolution of the Poisson equation and the continuity equations for the electrons and the holes. it calculates at all times and in all point of space in a sequence of finite elements, the concentration of electrons and holes and the value of the electrostatic potential [49].

The Poisson equation shows a relationship between the potential and the density of the carriers [49]:

$$\Delta V = \frac{-q}{\varepsilon}\,[\,p - n + N_D^{\;+} - N_A^{\;-}\,]. \tag{III.17}$$

Where **V** the potential, **q** the elementary charge of electrons, $\boldsymbol{\varepsilon}$ the dielectric constant, the $N_A^{\;-}$ and $N_D^{\;+}$ concentrations of ionized donor and acceptor dopants, and **n** and **p** the densities of electrons and holes.

The continuity equations for the electrons and the holes are [49]:

$$\frac{\partial n}{\partial t} = +\frac{1}{q}\,div\overrightarrow{J_n} + G_n - R_n\ . \tag{III. 18}$$

$$\frac{\partial p}{\partial t} = -\frac{1}{q}\,div\overrightarrow{J_p} + G_p - R_p\ \ . \tag{III. 19}$$

Or $\overrightarrow{J_n}$ and $\overrightarrow{J_P}$ are the current densities of electrons and holes, G_n and G_p generation rates for electrons is the holes, R_n and R_p recombination rates for electrons and holes.

Derivatives based on Boltzmann's transport theory have shown that the density of the currents in the continuity equations can be defined by the scattering training model. The current densities are expressed in two terms, the first corresponds to the entrainment of the charges by the electric field, the second corresponds to the diffusion of the carriers [49].

$$\overrightarrow{J_n} = qn\mu_n\vec{E} + qD_n\overrightarrow{gradn} \tag{III. 20}$$

$$\overrightarrow{J_p} = qp\mu_p\vec{E} + qD_p\overrightarrow{gradp} \tag{III. 21}$$

$$\vec{E} = -\overrightarrow{gradV} \tag{III. 22}$$

Or D_n and D_p are the diffusion coefficients. They are directly linked to the mobility of carriers through Einstein's relationship [49]:

$$D_n = \frac{K_B T}{q} \mu_n \qquad \text{(III. 23)} \qquad , \quad D_p = \frac{K_B T}{q} \mu_p \qquad \text{(III. 24)}$$

III.3. Silvaco Atlas Simulation Software

III.3.1.Definition

Atlas is a physically based two and three dimensional device simulator [50], which takes a two dimensional input structure which is specified and gridded by the user through an input program and solves the differential equations derived from Maxwell's laws to simulate the transport of carriers within the structure at each of the points of the grid. The user can specify any type of device using a large library of conductors, semiconductors and insulators, and can use solve statements to simulate the behavior of a device under certain conditions. The text input deckbuild, is used for the specification and solve statements of devices in this thesis. In deckbuild, users type input commands that first specify the structure and then set the conditions for simulating its behavior. These statements must follow a set structure to properly run the ATLAS software [48].

III.3.2.Atlas Inputs and Outputs

Atlas uses two types of input file [51]:

- A text file that contains Atlas commands.
- A structure file that defines the structure to be simulated.

Atlas produces three types of output files [51]:

- The runtime output that gives error and warning messages as the simulation proceeds.
- The log file that stores voltages and currents.
- The solution file that stores 2D and 3D data relating to the values of solution variables.

Figure.III.25, shows the types of information that flow in and out of Atlas.
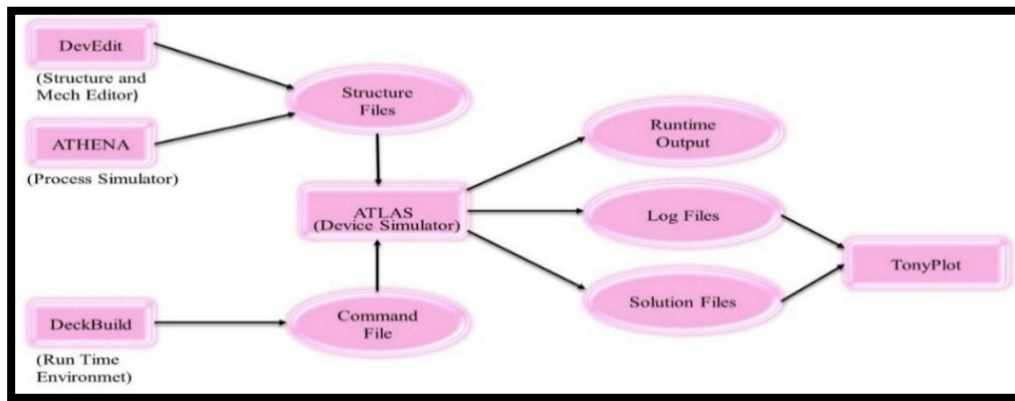
Figure.III.25: Atlas Inputs and Outputs [51].

ATLAS provides a comprehensive set of physical models, including [51]:

- ➢ DC, AC small-signal, and full time-dependency.
- ➢ Drift-diffusion transport models.
- ➢ Energy balance and Hydrodynamic transport models.
- ➢ Lattice heating and heat sinks.
- ➢ Graded and abrupt heterojunctions.
- ➢ Optoelectronic interactions with general ray tracing.
- ➢ Amorphous and polycrystalline materials.
- ➢ General circuit environments.
- ➢ Stimulated emission and radiation
- ➢ Fermi-Dirac and Boltzmann statistics.
- ➢ Advanced mobility models.
- ➢ Heavy doping effects.
- ➢ Full acceptor and donor trap dynamics
- ➢ Ohmic, Schottky, and insulating contacts.
- ➢ SRH, radiative, Auger, and surface recombination.
- ➢ Impact ionization (local and non-local).
- ➢ Floating gates.
- ➢ Band-to-band and Fowler-Nordheim tunneling.
- ➢ Hot carrier injection.
- ➢ Quantum transport models.
- ➢ Thermionic emission currents.

III.3.3.Running Atlas inside Deckbuild

To run Atlas inside Deckbuild we use the following command line [51]:

> Go Atlas.

III.4.Working with ATLAS

The development of the desired structure in Atlas is done using a declarative programming language. In the following, we give a brief overview on the construction and simulation of a structure in Atlas [51].

The Atlas input file contains a command line order. Each row consists of a number of statements that identifies the command and a set of parameters. The control groups are presented in Table .III.6 [51].

Table.III.6: Atlas command groups with the primary statements in each group [51].

Group	Statements
Structure Specification	Mesh
	Regions
	Electrodes
	Doping
Materials Model Specification	Material
	Models
	Contacts
	Interface
Numerical Method Selection	Method
Solution Specification	Log
	Solve
	Lead and save
Results analysis	Extract
	Tonyplot

III.4.1.Structure Specification

The structure specification is done by defining the mesh, the region, the electrodes and the doping levels [51].

III.4.1.1.Mesh

mesh width=5e04
x.mesh loc= 0   spac=100
x.mesh loc=980 spac=5
x.mesh loc=1020 spac=5
y.mesh loc=2000 spac=100
y.mesh loc= - 0.1 spac=0.02
y.mesh loc=0 spac=0.01
y.mesh loc=0.1 spac=0.001
y.mesh loc=5 spac=0.5
y.mesh loc=10 spac=0.5
y.mesh loc=10.05 spac=0.02

• The mesh is defined by a series of horizontal and vertical lines and the spacing between them. The mesh used for this thesis is two-dimensional. Therefore, only x and y parameters are defined. The mesh is created with the following statements[51] :
MESH SPACE.MULT=<VALUE>
X.MESH LOCATION=<VALUE>
SPACING=<VALUE>   Y.MESH
LOCATION=<VALUE> SPACING=<VALUE>

Figure.III.26, shows the mesh of the studied cell solar.
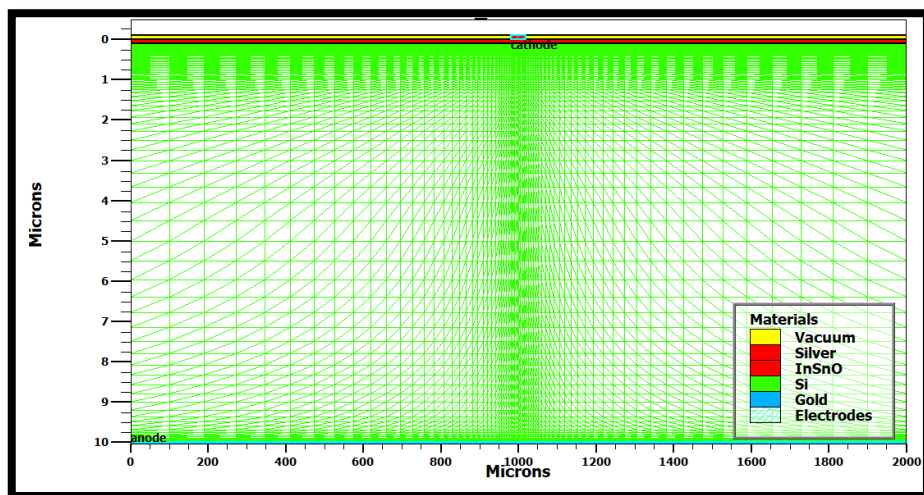
Figure.III.26: Atlas mesh.

III.4.1.2.Region

After mesh defined, the region is the next step [51]:

region num=1
material=silicon

x.min=0 x.max=2000
y.min=0.1 y.max=10

• The format to define the regions is as follows[51]:
  REGION number=<integer><material_type>
  /<position parameters>

Figure.III.27, shows regions generated by Atlas for the cell solar.
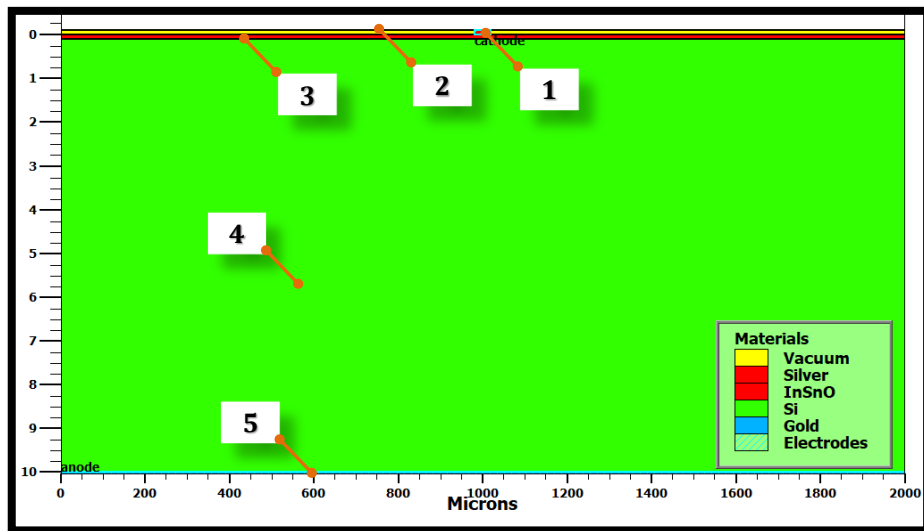
Figure.III.27: Atlas regions with materials defined.

- Region number one (1) is the front contact or cathode (silver in our study).

- Region number two (2) is the vacuum.

- Region number three (3) is the TCO (ITO, ZnO and TiO_2)

- Region number four (4) is the crystalline silicon.

- Region number five (5) is the back contact or anode (gold in our study).

III.4.1.3.Electrodes

electrode   num=1
name=anode x.min=0
x.max=2000 y.min=10
y.max=10.05 material=gold

electrode   num=2
name=cathode x.min=980
x.max=1020 y.min=0
y.max=0.1 material=silver

• Typically, in this simulation the only electrodes defined are the anode and the cathode. However, Silvaco Atlas has a limit of 50 electrodes that can be defined. The format to define electrodes is as follows[51] : ELECTRODE NAME=<electrode name><position_parameters>.

An example of created electrodes can be found in Figure.III.28.
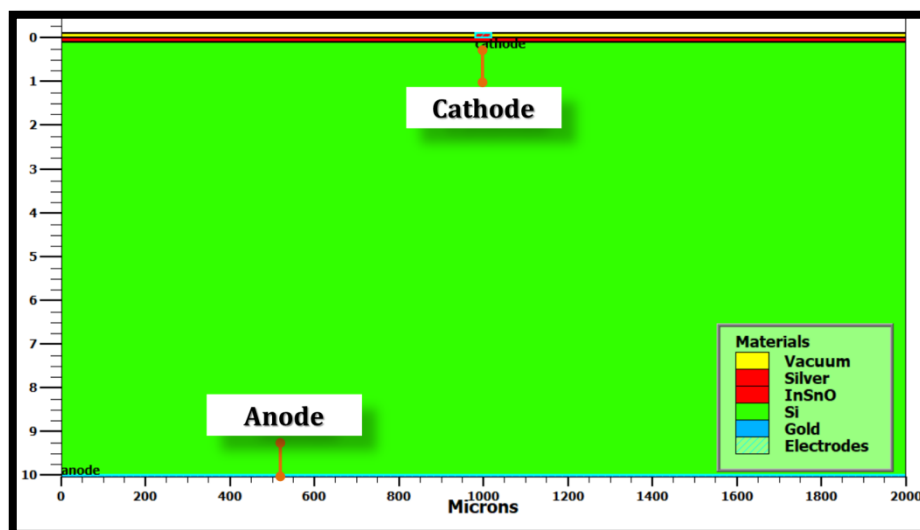
Figure III.28: Atlas electrodes.

III.4.1.3.Doping

After Electrodes defined, the doping is the next step [50,52].

doping uniform concentration =1e17
n-type region=2

doping uniform concentration=1e14

p-type region=3

- After creating the separate regions and assigning materials to those regions, the materials themselves can be doped. The user specifies the doping using the DOPING statement[51]:
- The DOPING statement is broken down into three sections. First, the distribution type can be either uniform, Gaussian, or complementary error function forms. Next, a concentration and type of doping must be specified. Finally, the region to be doped must be identified[51] : DOPING<distribution_type><dopant_type><position_parameters>.

From Figure.III.29, the doping types and the doping levels are defined. Doping can be n type or p type.
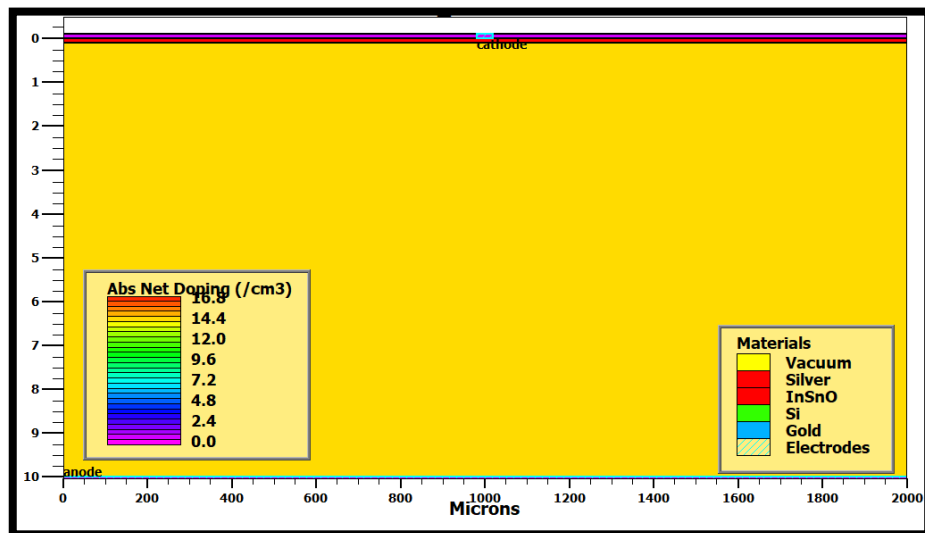
Figure.III.29: The doping distribution in regions.

III.4.2.Materials Model Specification

After the structure specification, the materials model specification is the next step [51] **.**

III.4.2.1.Material

material material=InSnO
user.group=semiconductor
user.default=ITO Eg300=3.75
affinity=4.8 mun=45 mup=0.45
Nc300=5.8e18 Nv300=1e18
permittivity=8.9 index.file=ITO-nk.txt

- The format for the material statement is as follows[51] :
  MATERIAL<localization><material_definition>

III.4.2.2.Models

The physical models fall into five categories: mobility, recombination, carrier statistics, impact ionization, and tunneling. The syntax of the model statement is as follows [51]:

MODELS <model-name>

The choice of model depends on the materials chosen for simulation. In our study, we use the simplest model:

Models srh print

Specifies Shockley-Read-Hall recombination using fixed lifetimes [51].

III.4.2.3.Contact

Silver (Cathode)

contact name=cathode workfunction=4.21

gold (Anode)

contact name=anode workfunction=5.23

- Contact determines the attributes of the electrode. The syntax for contact is as follows[51] :
  CONTACT NAME=<ename> (workfunction)

III.4.2.4.Interface

interface x.min=0 x.max=2000
y.min=0 y.max=0 s.n=1e3 s.p=1e3

interface x.min=0   x.max=2000
y.min=10 y.max=10 s.n=1e15
s.p=1e5

• The semiconductor or insulator boundaries
  are determined with the interface statement.
  The syntax is as follows[51]:
• INTERFACE{<parameters>}

III.4.3.Numerical Method Selection

There are various numerical methods to calculate solutions to semiconductor device problems.
The syntax of the method statement is as follows [51]:

METHODS <methode-name>

 In our study, we use the following method:

NEWTON:

Can solves the total system of
unknowns together.

TRAP:

It is a method more accurate than
newton that depends on the
division of the given step in case
the solution does not converge.
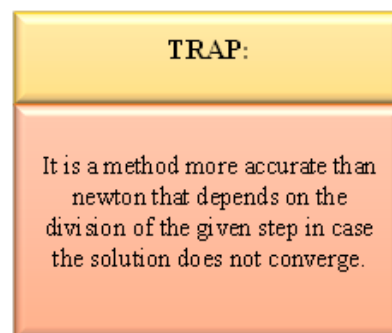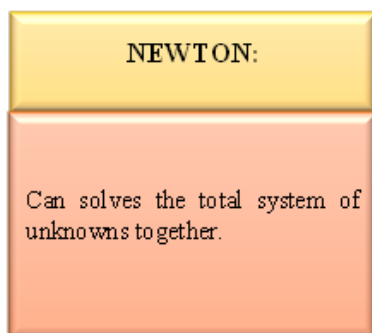
III.4.4.Solution Specification

After completing the numerical method selection, the solution specification is next. Solution
specification is broken down into log, solve, load, and save statements [51]:

log outfile=IVlight.log

- Log files (.log) store the terminal characteristics calculated by Atlas. These are current and voltages at electrodes in DC simulations. In transient simulations, the time is stored. In AC simulations, the small signal frequency, the conductances and capacitances are saved. The following shows an example of the LOG statement[51].
LOG OUTFILE=myoutputfile.log
The example saves the current-voltage information into myoutputfile.log .

solve vanode=0 vstep=0.01 vfinal=0.4 name=anode

solve vanode=0.4 vstep=0.01 vfinal=1 name=anode

solve b1=1

- The SOLVE statement follows the LOG statement. SOLVE performs a solution for one or more bias points [51].

save outfile=solar.str

- The SAVE statement enters all node point information into an output file.
- The following are examples of SAVE statements[51]:
SAVE OUTF=SOL.STR
In this case, SOL.STR has information saved after a SOLVE statement.

III.4.5.Data Extraction and Plotting

Once a solution has been found for a semiconductor device problem, the information can be displayed graphically with Tonyplot. Additionally, device parameters can be extracted with the EXTRACT statement [51].

extract name="Isc [mA/cm^2]" y.val from curve (v."anode",i."cathode"*1e3) where x.val=0.0
extract name="Voc" x.val from curve (v."anode",i."cathode"*1e3) where
y.val=0.0

• The TONYPLOT statement is[51] : TONYPLOT "<filename>".

Plotting Current Density versus Voltage and Electric Field Curves
tonyplot Cell_conv2ini.str -set solardril.set
tonyplot IVcurvlight.dat
outfile="powerlight.dat"

• The EXTRACT statement is[51] : EXTRACT INIT INF="<filename>".

III.4.6.Illumination

beam num=1 x.origin=1000 y.origin=-30 angle=90.0 power.file=cdrom.spec reflects=1 front.refl back.refl quantum.eff=1.0

• this statement defines the numder of the light beams,the origin of the radius,the x and y corrdinates of the origin of the light beam microns ,the incidence angle,and the reflection number of the light beam on the front and rear layer, the quantum efficiency[51] .

III.5.Results and discussions

III.5.1.Simulation parameter

The device material input parameters used in this simulation are given in Table.III.7 and Table. III.8.

Table.III.7: Physical parameters used in the simulation.

Parameter	Designation	ITO [11,53]	ZnO [54]	TiO₂ [55]	Si [55]
$E_g(eV)$	Gap energy	3.75	3.4	3.2	1.12
$e\chi_s(eV)$	Affinity	4.8	4.5	4.1	4.17
$N_c(cm^{-3})$	Effective density of Conduction band ($\times 10^{19}$)	0.58	1	20	2.8
$N_v(cm^{-3})$	Effective density of Valence band ($\times 10^{19}$)	0.1	0.1	10	1.04
$\mu_n(cm^2V^{-1}s^{-1})$	Electron mobility	45	150	0.3	1000
$\mu_p(cm^2V^{-1}s^{-1})$	Hole mobility	4.5	28	0.1	500
ε_r	Relative dielectric constant	8.9	8.66	12.3	12.8

Table.III.8: Physical parameters used in the simulation for solar cell with buffer layer formed between TCO and Si.

Parameter	ITO/Si [53]	ZnO/Si [56]	TiO₂/Si [57]
$E_g(eV)$	2.4	2.24	2.14
$e\chi_i(eV)$	4.48	4.33	4.1
$N_c(\times 10^{19}cm^{-3})$	1.7	1.9	11.4
$N_v(\times 10^{19}cm^{-3})$	0.57	0.57	5.52
$\mu_n(cm^2V^{-1}s^{-1})$	45	150	0.3
$\mu_p(cm^2V^{-1}s^{-1})$	4.5	28	0.1
ε_r	10	10	10

III.5.2.Results and discussions

We notice that this study is carried out in the ideal case by omitting defects in the solar cell and we began by the ITO(n-type)/Si(p-type) solar cell. The first structure named structure 1 is presented in Figure.III.30, in which the cathode material is the silver. We have tried to improve

structure 1 to structure 2 in which an SiO₂ anti-reflecting (AR) layer is added on the top of the cell and the silver cathode is replaced by three transparent conductor ITO cathode as shown in Figure.III.31.
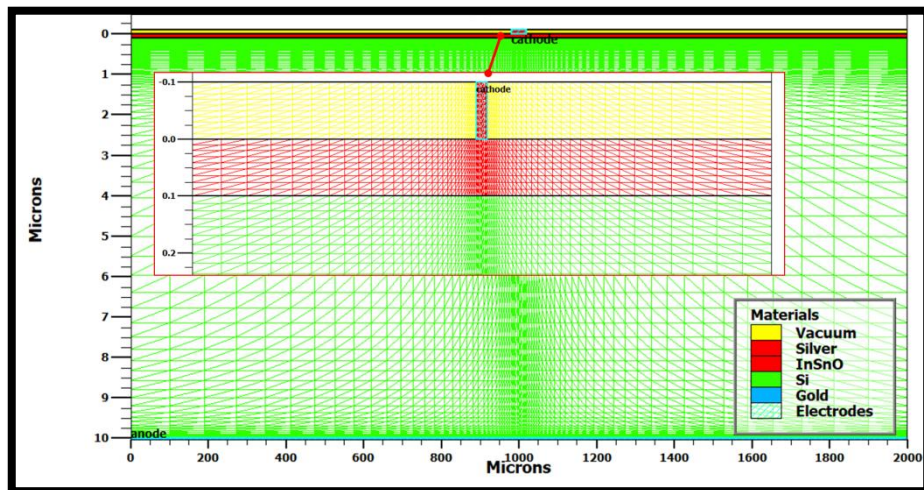
Figure.III.30: ITO(n-type)/Si(p-type) structure with silver cathode.
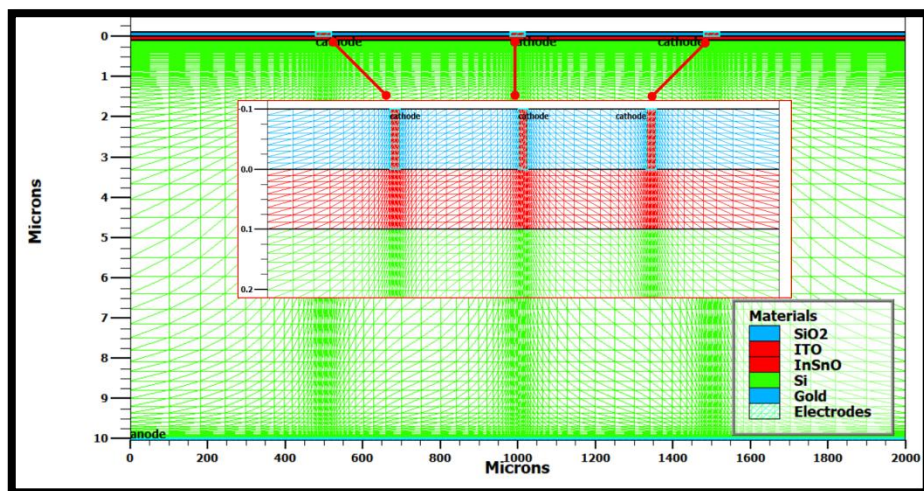
Figure.III.31: ITO(n-type)/Si(p-type) structure with three cathode of ITO.

Figure.III.32, shows the calculated J-V characteristics. From Table.III.9, by comparing the two structures indeed there is improvement in J_{sc} unlike V_{oc} and FF that increase a little. Structure 2 exhibits a conversion efficiency of 3.14% better than 0.85% of structure 1. These values are in the experimental range (early measurement without any optimized conditions).

60
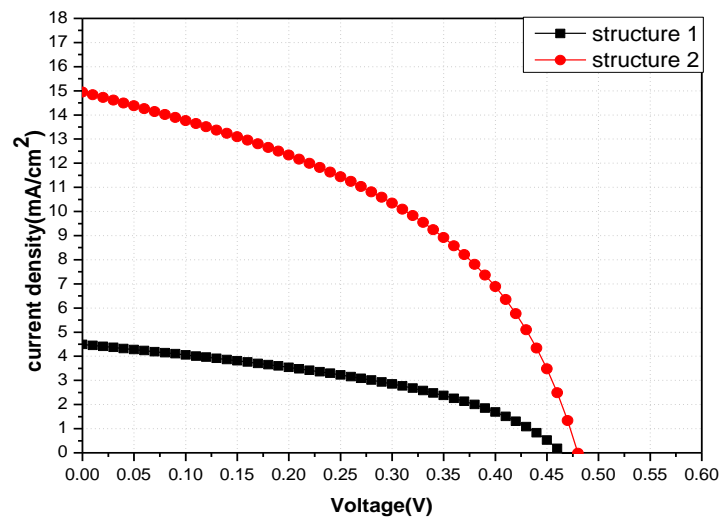
Figure.III.32: The calculated J-V characteristics of structure 1 and structure 2.

Table.III.9: The calculated output parameters of the ITO(n-type)/Si(p-type) solar cell.

Cell thickness 10 µm	$J_{sc}(mA/cm^2)$	$V_{oc}(V)$	FF	$\eta\%$
Structure -1-	4.49	0.464	0.411	0.85
Structure -2-	14.94	0.479	0.439	3.14

III.5.2.1.Effect of Si thickness

In this section, we study the thickness effect of the C-Si p-layer. The layer thickness is varied from 10 µm to 500 µm using structure 2. The calculated J-V characteristics are presented in Figure.III.33, and the electrical outputs are summarized in Figure.III.34.

From Figure.III.34, significant increase is noticed in J_{sc} from 14.94 mA/cm^2 to 29.47 mA/cm^2 with saturation like behavior that starts at 300 µm. All the other parameters also increase, FF from 0.439 to 0.531, V_{oc} from 0.479 V to 0.505 V and the efficiency from 3.14% to 7.9 %.

The significant increase in J_{sc} is related to the absorption with the augmentation of the p-layer thickness but without exceeding the free carrier diffusion length.
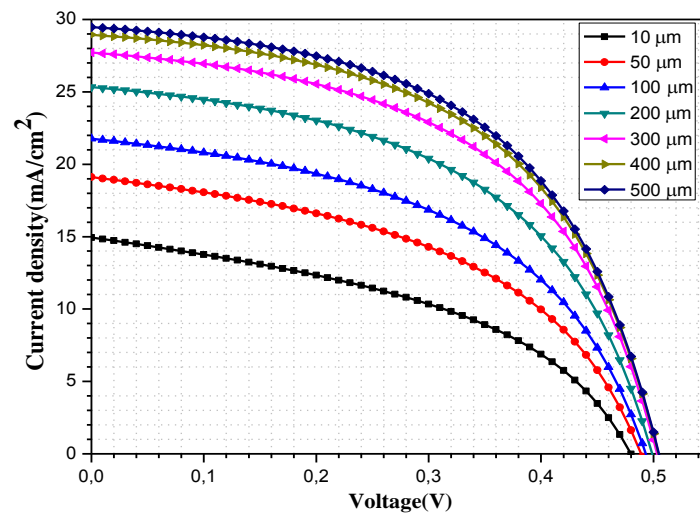
Figure.III.33: Effect of p-layer (Si) thickness on the J-V characteristic.
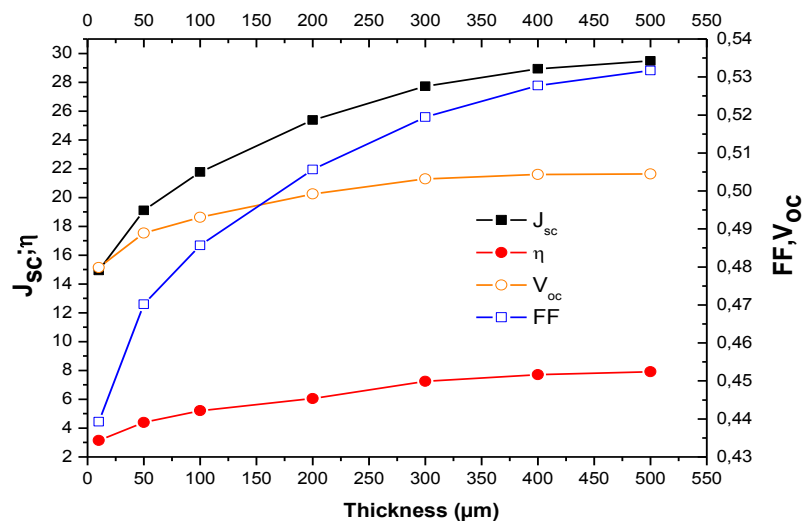
Figure.III.34: Effect of p-layer (Si) thickness on output parameters.

III.5.2.2.Effect of the ITO layer thickness

The p-type C-Si layer thickness is kept at 500 μm, and thickness of ITO ranges from 0.1 to 1μm. The J-V characteristics are presented in Figure.III.35, and the extracted outputs are summarized in Figure.III.36.
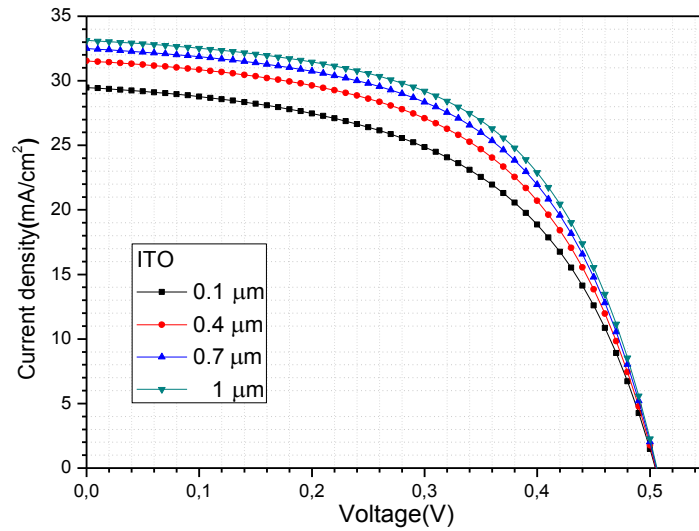
Figure.III.35: Effect of n-layer (ITO) thickness on the J-V characteristic.

From Figure.III.36, it is observed that V_{oc} remains constant during the simulation process while FF increases from 0.531 to 0.564. The value of J_{sc} is found to increase and saturates with a few values from 29.47 mA/cm^2 to 33.13 mA/cm^2. The efficiency enhances from 7.9% to 9.45%. The little increase remarked in J_{sc} is because the ITO is characterized by transparency and then absorbs in the UV and generates few carriers.

Since the saturation feature is apparent from 0.4 µm, it is not necessary to increase the thickness to more than 1 µm. Usually the TCO are deposited in the form of thin layers, that is to say that their thickness ranges from a few nanometres to a few micrometres.
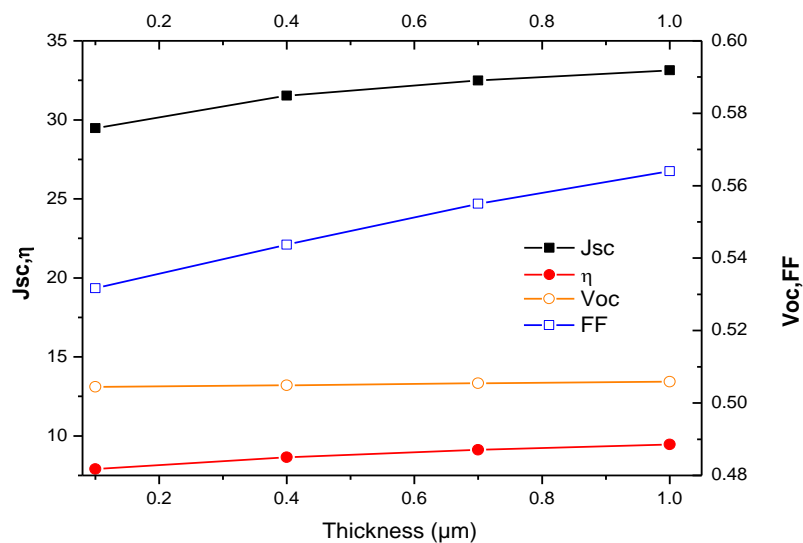
Figure.III.36: Effect of n-layer (ITO) thickness on output parameters.

III.5.2.3. ITO (n-type)/Si (p-type) layer doping effect

In this section the doping of the two layer of the cell is augmented and in addition a back doping in the Si region is inserted. The obtained results are summarized in Table.III.10.

Table.III.10: The calculated output parameters of the ITO (n-type)/Si (p-type) solar cell with variation doping.

ITO(1µm)/Si(500µm) Doping (cm^{-3})	$J_{sc}(mA/cm^2)$	$V_{oc}(V)$	FF	$\eta\%$
ITO $N_d = 1 \times 10^{17}$	33.13	0.505	0.564	9.45
ITO $N_d = 5 \times 10^{18}$	34.06	0.506	0.654	11.29
Si $N_a = 5 \times 10^{15}$	32.33	0.586	0.803	15.25
Si $N_a = 5 \times 10^{16}$	32.23	0.646	0.826	17.22
Back Si $N_a = 5 \times 10^{18}$	32.26	0.646	0.826	17.24

A benefit effect of the doping is observed in FF and V_{oc} unlikely to J_{sc} which reaches 34.06 mA/cm^2 only with the emitter doping increase. The best efficiency is 17.24 % using a back doping of $5 \times 10^{18} cm^{-3}$. It is reminded that these values are obtained in the ideal case when the defects in the structure are neglected. In addition, it is possible to change this heavy doped back Si layer by hole selective TCO to avoid issues associated with heavy doping cost and treatment this can be a perspective for future works.

III.5.2.4.Anode work function effect

In Figure.III.37, is presented the band gap equilibrium of the ITO/Si structure with thicknesses and doping adopted in the previous section. It is clear that an ohmic contact is established in front between ITO (n) layer and the semi-metallic ITO cathode as well as at the rear contact between the heavily doped Si layer and the anode gold. However, if the ITO (n) form a good barrier to block hole and assure an efficient selectivity of electrons, the heavily doped Si present a weak barrier for electrons created in p-Si layer (dominant layer for absorption and photo-generation). Therefore the effect of anode work function is studied in this section for more efficient separation between electrons and holes in the back of the structure.
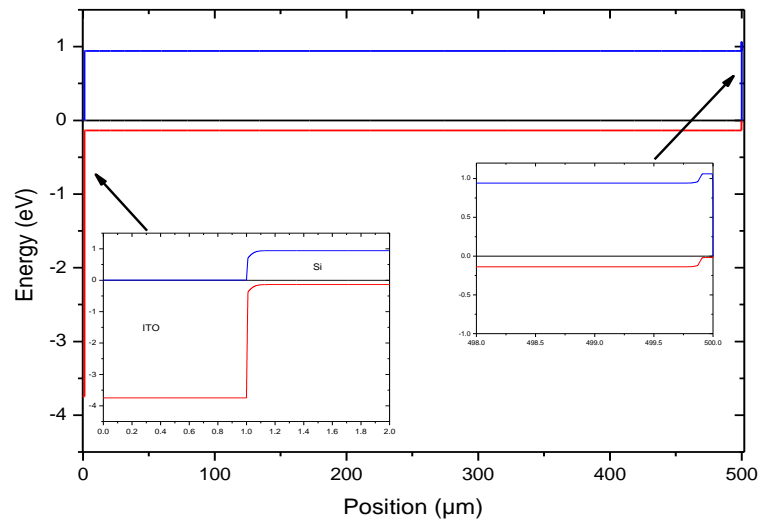
Figure III.37: Band gap diagram at thermodynamic equilibrium.
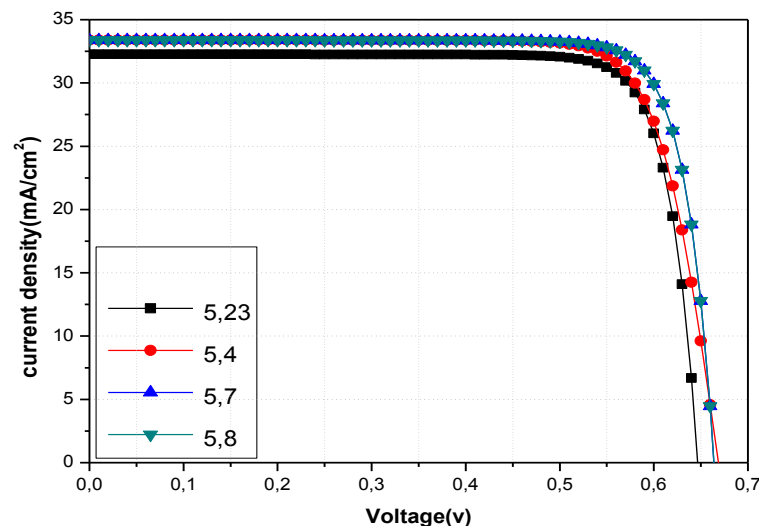
Figure.III.38: J-V characteristics for different anode work function values**.**

We expect that the cathode work function has no effect on hole selectivity since the barrier established by ITO in front of them is very high and this is what we have remarked indeed in simulation. Consequently, the effect of cathode work function has been neglected.

The work function anode contact is changed from 5.23 eV to 5.8 eV, taking into account the precedent optimum parameters of thicknesses and doping. The obtained J-V characteristics are presented in Figure.III.38, and the extracted outputs are summarized in Table.III.11.

Table.III.11: The calculated output parameters of the ITO (n-type)/Si (p-type) solar cell with variation metal work function for the back contact.

Work function (eV)	$J_{sc}(mA/cm^2)$	$V_{oc}(V)$	FF	$\eta\%$
$5.23\ eV$	32.26	0.646	0.826	17.24
$5.4\ \ eV$	32.82	0.653	0.828	17.73
$5.7\ \ eV$	33.38	0.663	0.830	18.39
$5.8\ eV$	33.38	0.663	0.830	18.39

From the obtained results, it is observed that all outputs improve little a bit with the increase of the anode and the reached efficiency is 18.39%. Theoretically platinum with work function around 5.65~6eV as anode material gives the best efficiency. However, in practice it not suitable to use it since it is more expensive than gold.

III.5.2.5.Buffer layer effect

In this section we suggest the formation of a buffer layer between the ITO and Si region as shown in Figure.III.39. The chosen input parameters of this buffer layer are given in the beginning of the result section (Table.III.8). The J-V characteristic obtained with the buffer layer is compared to the original and without the buffer layer in Figure.III.40, and the outputs are presented in Table.III.12.
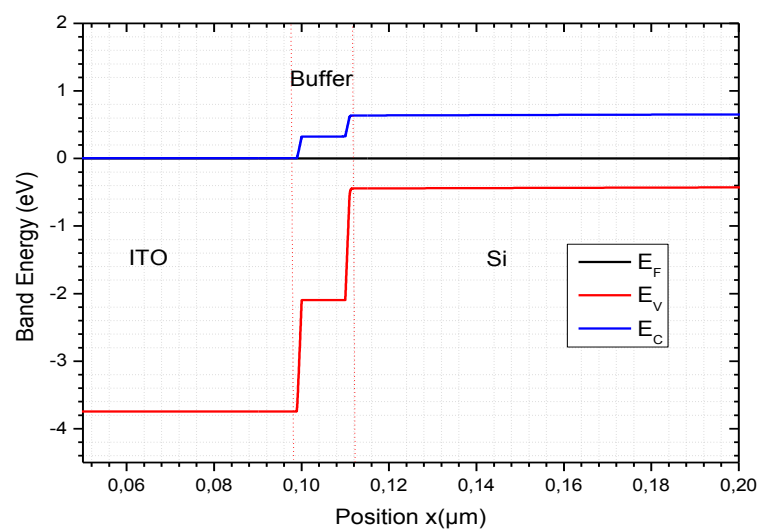
Figure.III.39: Buffer layer inserted between ITO and Si.
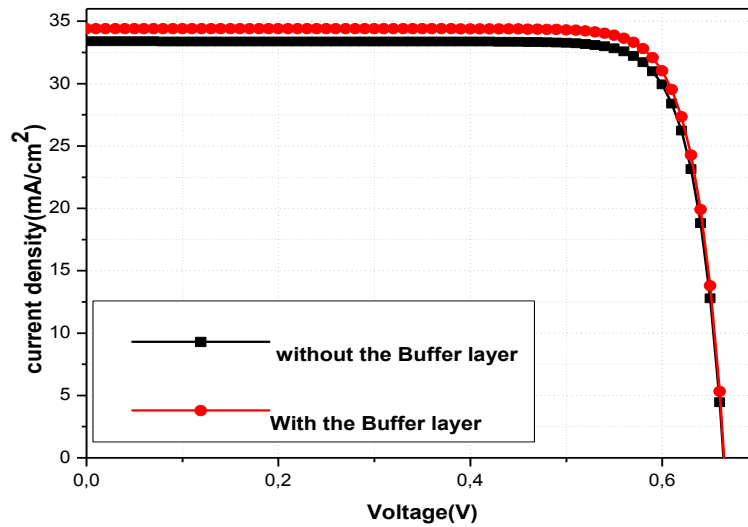
Figure.III.40: The J-V characteristic with and without the buffer layer.

Table.III.12: Effect of the buffer layer

	$J_{sc}(mA/cm^2)$	$V_{oc}(V)$	FF	$\eta\%$
Without buffer layer	33.38	0.663	0.830	18.39
With buffer layer	35.01	0.665	0.832	19.39

Little amelioration is noticed in all outputs mainly the current J_{sc}, and the efficiency becomes 19.39% compared to 18.39% without the buffer layer.

III.6. Comparison between ITO/Si, ZnO/Si and TiO₂/Si

In this section, ITO is replaced by ZnO and TiO_2. The obtained J-V properties are shown in Figure III.41, Figure III.42 and Figure III.43, for cells before improvement and then without and with buffer layer respectively. Table III.13 and Table III.14 summarizes the outputs extracted.
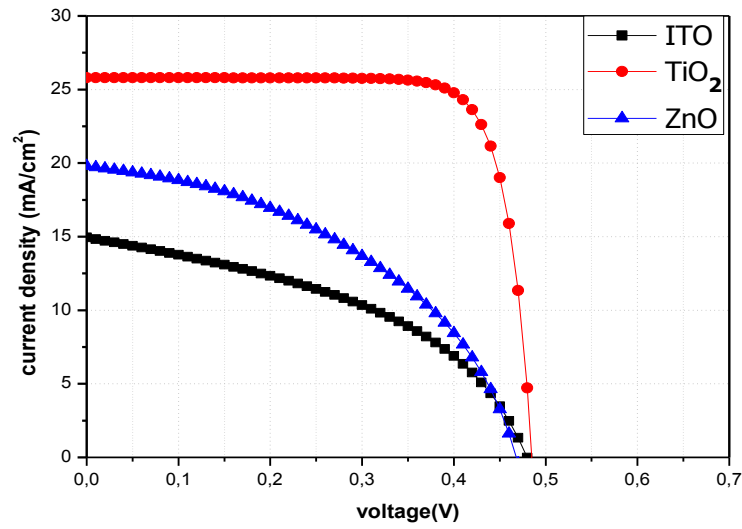
Figure III.41: Comparison between J-V characteristics of ITO/Si, ZnO/Si and TiO₂ /Si solar cell before optimization.
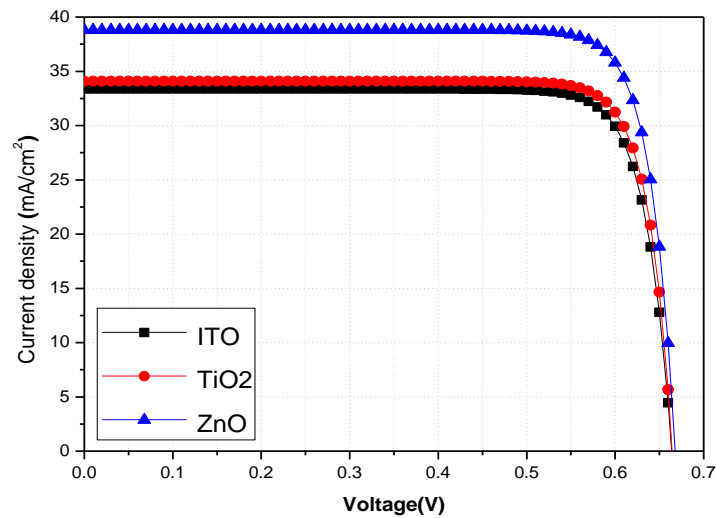
Figure.III.42: Comparison between J-V characteristics of ITO/Si, ZnO/Si and TiO₂ /Si solar cell without buffer layer.
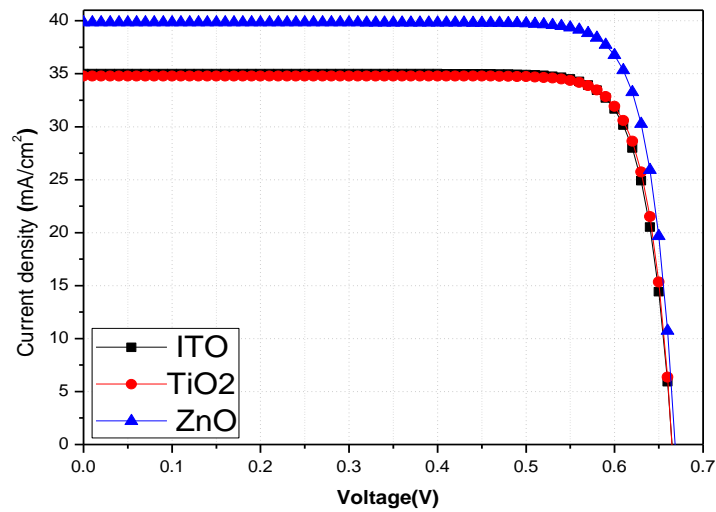
Figure III.43: Comparison between J-V characteristics of ITO/Si, ZnO/Si and TiO₂ /Si solar cell with buffer layer.

Table.III.13: The calculated output parameters of ITO/Si, ZnO/Si and TiO₂ /Si solar cells before optimizations.

Cell thickness10 μm	$J_{sc}(mA/cm^2)$	$V_{oc}(V)$	FF	$\eta\%$
ITO/Si	14.94	0.479	0.439	3.14
ZnO/Si	19.80	0.468	0.444	4.11
TiO$_2$/Si	25.80	0.484	0.796	9.96

Table.III.14: The calculated output parameters of ITO/Si, ZnO/Si and TiO₂ /Si solar cells after optimization without and with the buffer layer.

Cell thickness 500 μm	$J_{sc}(mA/cm^2)$	$V_{oc}(V)$	FF	$\eta\%$
ITO/Si	33.38	0.663	0.830	18.39
ZnO/Si	38.91	0.667	0.837	21.78
TiO$_2$/Si	34.09	0.664	0.839	19.00
With a buffer layer	$J_{sc}(mA/cm^2)$	$V_{oc}(V)$	FF	$\eta\%$
ITO/Si	35.01	0.665	0.832	19.39
ZnO/Si	39.81	0.668	0.838	22.30
TiO$_2$/Si	34.78	0.664	0.839	19.41

From results, before optimization TiO$_2$/Si shows the best efficiency of 9.96% while after optimization ZnO/Si has the best output parameters compared with ITO/Si and TiO$_2$/Si where the efficiency reaches 21.78% without a buffer layer and 22.30% with a buffer layer. For ITO/Si and TiO$_2$/Si the obtained results are very close without and with buffer layer.

The best results with ZnO can be related to an extended barrier established in C-Si at the side of the buffer layer in addition to the abrupt barrier at the interface, as presented in Figure.III.44. However, TiO$_2$ (Figure.III.45) is similar to ITO with only abrupt interface with the buffer layer.
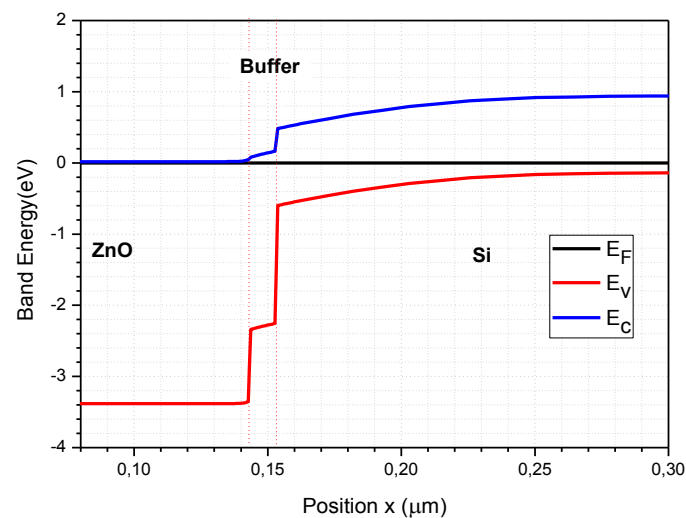
Figure.III.44: Energy diagram of ZnO/buffer/Si heterojunction solar cell.
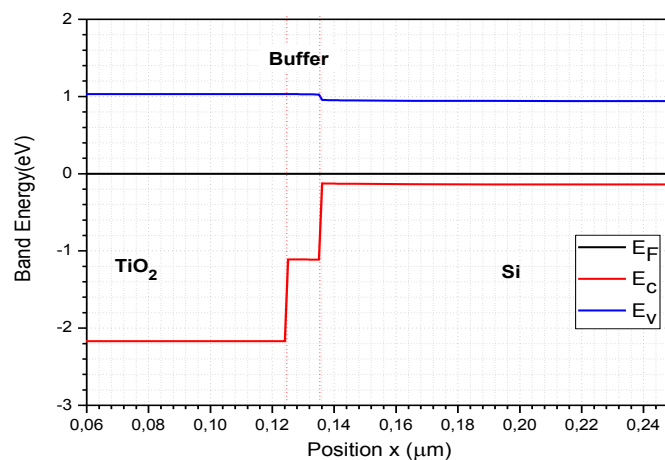
Figure.III.45: Energy diagram of TiO$_2$/buffer/Si heterojunction solar cell.

III.7. Conclusion

In this chapter, we have successfully simulated solar cells based on TCO (n)/Si (p) using Silvaco-Atlas software. The effect of several parameters has been presented which are the type of TCO, thickness and doping of each layers, work function of anode, and the insertion of a buffer layer between TCO and Si. Before optimizations, the calculated conversion efficiency of ITO/Si, ZnO/Si and TiO_2 /Si respectively, was 3.14%, 4.11% and 9.96%. After optimization process the ITO/Si cell efficiency reached 19.39% with a buffer layer inserted at ITO/Si interface. Replacing ITO with ZnO and TiO_2, the obtained efficiency was 22.30% and 19.41% respectively. Then we conclude that the best material as electron selective TCO in heterojunction C-Si solar cell is ZnO.
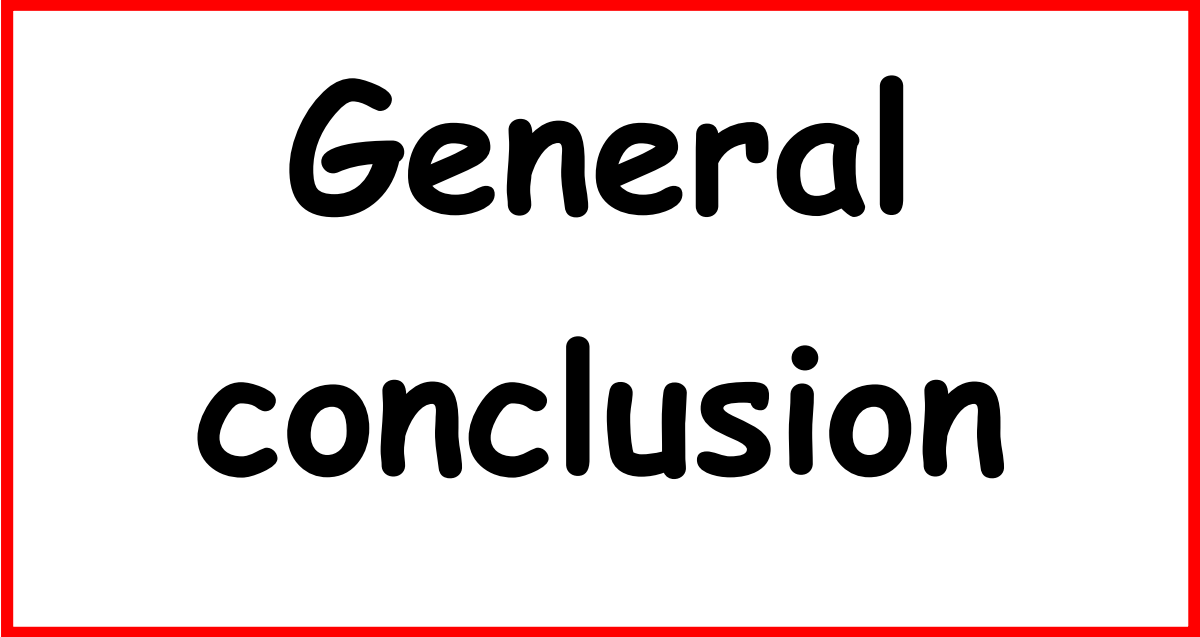
General conclusion
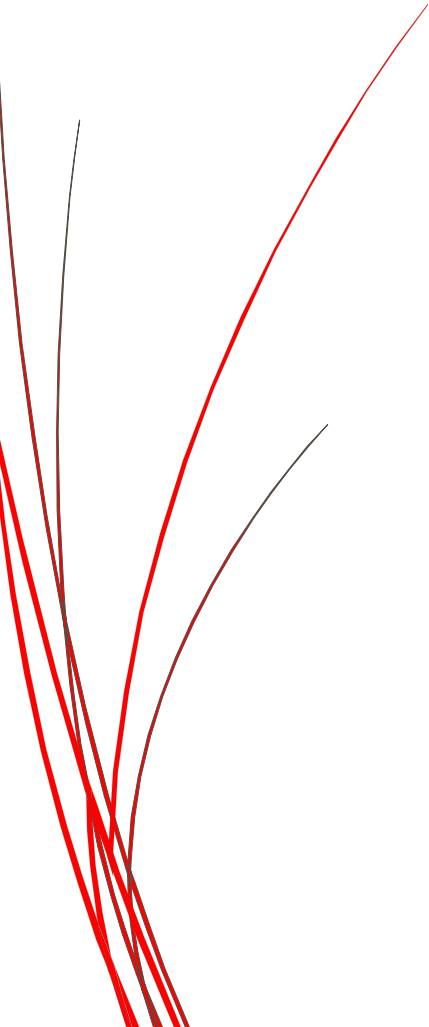
General conclusion

In this work, we have achieved a numerical simulation of heterojunction solar cells based on conductive oxide/Si heterojunction, the proposed cells are: ITO/Si, ZnO/Si and TiO$_2$ /Si by Silvaco-Atlas software.

In the optimization process different parameters have been changed which are thickness and doping of each layers composed the cells, the workfunction of anode, and finally we study the effect of buffer layer. The simulated curves are the J-V characteristic and the output parameters of the solar cell: the short circuit current (J_{SC}), the open circuit voltage (V_{oc}) , the fill factor (FF), the power conversion efficiency (η). The main results obtained from simulations using Silvaco-Atlas can be summarized as follows:

> ➢ The increase of the p-layer (Si) and n-layer (TCO) thickness lead to an increase in short circuit current (J_{SC}) and in power conversion efficiency (η) . Changes in fill factor (FF) and open circuit voltage (V_{oc}) can be ignored.
> ➢ The increase of n-layer (TCO) doping lead to an increase in J_{SC} and η.
> ➢ The increase of p-layer (Si) doping lead to an increase in η and decrease in Jsc, and when p-layer (Si) has back doping lead to an increase in η and constancy V_{oc} and FF.
> ➢ The increase in the anode work function leads to an increase in the output parameters. The optimum obtained efficiency corresponds to platinum (Pt) as anode.
> ➢ The effect of buffer layer leads to an increase in the output parameters especially J_{SC} and η.

The above results are related to all employed TCO: ITO, ZnO and TiO$_2$. After the improvement process the cell efficiency reaches 19.39% for ITO/Si, 22.30% for ZnO/Si and 19.41% TiO$_2$/Si and the best TCO (n) is consequently ZnO.

REFERENCES

[1]   G. V. Samsonov, *The oxide handbook*: Springer Science & Business Media, 2013.

[2]   I.Jellal, H. Ahmoum, Y. Khaaissa, K. Nouneh, M. Boughrara, M. Fahoume, ·S. Chopra, J. Naja4, "Experimental and ab‑ initio investigation of the microstructure and optoelectronic properties of FCM–CVD‑ prepared Al‑ doped ZnO thin films", Applied Physics A 125:650, 2019.

[3]   Raisul Islam, Pranav Ramesh, Ju Hyung Nam and Krishna C. Saraswat, "Nickel Oxide Carrier Selective Contacts for Silicon Solar Cells" 978-1-4799-7944-8/15/$31.00 ©2015 IEEE.

[4]   M. Ouafa and C. Amar, "Etude et simulation des cellules solaires à hétérojonctions de type ITO/Si," Université Mouloud Mammeri, 2016.

[5]   B. Chavillon, "Synthèse et caractérisation d'oxydes transparents conducteurs de type p pour application en cellules solaires à colorant," 2011.

[6]   Ref&1 :Érica Pereira da Silvaa, Michel Chavesa, Steven Frederick Durranta, Paulo Noronha Lisboa-Filhob, José Roberto Ribeiro Bortoleto, "Morphological and Electrical Evolution of ZnO:Al Thin Films Deposited by RF Magnetron Sputtering onto Glass Substrates", Materials Research. 2014; 17(6): 1384-1390.

[7]   N. Manavizadeh, F. A. Boroumand, E. Asl-Soleimani, F. Raissi, S. Bagherzadeh, A. Khodayari, and M. A. Rasouli, "Influence of substrates on the structural and morphological properties of RF sputtered ITO thin films for photovoltaic application," *Thin Solid Films,* vol. 517, pp. 2324-2327, 2009.

[8]   A. El Hichou, A. Kachouane, J. Bubendorff, M. Addou, J. Ebothe, M. Troyon, and A. Bougrine, "Effect of substrate temperature on electrical, structural, optical and cathodoluminescent properties of In2O3-Sn thin films prepared by spray pyrolysis," *Thin Solid Films,* vol. 458, pp. 263-268, 2004.

[9]   X. Zhang, W. Wu, T. Tian, Y. Man, and J. Wang, "Deposition of transparent conductive mesoporous indium tin oxide thin films by a dip coating process," *Materials Research Bulletin,* vol. 43, pp. 1016-1022, 2008.

[10]   I. Elfallal, R. Pilkington, and A. Hill, "Formulation of a statistical thermodynamic model for the electron concentration in heavily doped metal oxide semiconductors applied to the tin-doped indium oxide system," *Thin Solid Films,* vol. 223, pp. 303-310, 1993.

[11]   L. Gupta, A. Mansingh, and P. Srivastava, "Band gap narrowing and the band structure of tin-doped indium oxide films," *Thin Solid Films,* vol. 176, pp. 33-44, 1989.

[12]   A. Khodorov, M. Piechowiak, and M. Gomes, "Structural, electrical and optical properties of indium–tin–oxide thin films prepared by pulsed laser deposition," *Thin Solid Films,* vol. 515, pp. 7829-7833, 2007.

[13]   M. H. Habibi and N. Talebian, "The effect of annealing on structural, optical and electrical properties of nanostructured tin doped indium oxide thin films," *Acta Chim. Slov,* vol. 52, pp. 53-59, 2005.

[14]   D.-J. Won et al, « Effects ofthermally induced anatase-to-rutile phase transition in MOCVD-grown TiO2 films on structural and optical properties», Appl. Phys, vol. 73, (2001), 595–600.

[15] J. Ederth, "Electrical transport in nanoparticle thin films of gold and indium tin oxide," Acta Universitatis Upsaliensis, 2003.

[16] F. Hadjersi, "Investigation des propriétés structurales, optiques et électriques des films ITO élaborés par pulvérisation cathodique RF: effet du recuit," 2018.

[17] S. A. Bashar, "Study of indium tin oxide (ITO) for novel optoelectronic devices," *UMIST, Manchester*, pp. 106-109, 1998.

[18] K. Daoudi, "ÉLABORATION ET CARACTERISATION DE FILMS MINCES D'OXYDE D'INDIUM DOPE A L'ETAIN OBTENUS PAR VOIE SOL-GEL Potentialité pour la réalisation d'électrodes sur silicium poreux," 2003.

[19] V. Malathy, S. Sivaranjani, V. Vidhya, J. J. Prince, T. Balasubramanian, C. Sanjeeviraja, and M. Jayachandran, "Amorphous to crystalline transition and optoelectronic properties of nanocrystalline indium tin oxide (ITO) films sputtered with high rf power at room temperature," *Journal of non-crystalline solids*, vol. 355, pp. 1508-1516, 2009.

[20] S. Mahmoudi, "Etude des nanoparticules de dioxyde de titane élaborées par voies chimiques," 2014.

[21] Y. BOUACHIBA, "Contribution à l'élaboration de l'oxyde de titane par le procédé sol-gel: Effet du dopage et des conditions expérimentales," Université de Constantine 1, 2014.

[22] C.-P. Lin, H. Chen, A. Nakaruk, P. Koshy, C.C. Sorrell, "Effect of Annealing Temperature on the Photocatalytic Activity of TiO2 Thin Films", Energy Procedia 34 (2013) 627 − 636.

[23] S. Bouhadoun, "Synthèse de nanoparticules de dioxyde de titane par pyrolyse laser et leur application en photocatalyse," 2015.

[24] A. Hajjaji, M. Amlouk, M. Gaidi, B. Bessais, and M. A. El Khakani, *Chromium doped TiO2 sputtered thin films: synthesis, physical investigations and applications*: Springer, 2014.

[25] J. Wang, "Nanoparticules à base d'oxyde de titane par pyrolyse laser: synthèse, proprietés et application au photovotaïque," Paris 11, 2014.

[26] G. F. Knoll, *Radiation detection and measurement*: John Wiley & Sons, 2010.

[27] H. Kitaguchi, H. Miyai, S. Izumi, and A. Kaihara, "Silicon semiconductor detectors for various nuclear radiations," *IEEE Transactions on Nuclear Science*, vol. 43, pp. 1846-1850, 1996.

[28] H. Taylor and M. Goldhaber, "Detection of nuclear disintegration in a photographic emulsion," *Nature*, vol. 135, pp. 341-341, 1935.

[29] E. B. Flom, M. Li, A. Acero, N. Maskil, and S. A. Rice, "In-plane structure of the liquid-vapor interface of an alloy: a grazing incidence X-ray diffraction study of bismuth: gallium," *Science*, vol. 260, pp. 332-335, 1993.

[30] S. Fichtner, T. Reimer, S. Chemnitz, F. Lofink, and B. Wagner, "Stress controlled pulsed direct current co-sputtered Al1− xScxN as piezoelectric phase for micromechanical sensor applications," *APL Materials*, vol. 3, p. 116102, 2015.

[31] C. Kittel, "Introduction à la physique de l'état solide: maîtrise de physique," 1972.

[32] D. K. Schroder, *Semiconductor material and device characterization*: John Wiley & Sons, 2015.

[33] M. Soylu and F. Yakuphanoglu, "Photovoltaic and interface state density properties of the Au/n-GaAs Schottky barrier solar cell," *Thin Solid Films*, vol. 519, pp. 1950-1954, 2011.

[34] L. A. Green, *Silicon solar cells: advanced principles & practice*: Centre for Photovoltaic Devices and Systems, 1995.

[35] A. Redha, "Etude de l'interaction électron-matière des nanostructures de l'arséniure de gallium," *université Mentouri Constantine,* 2011.

[36] Babar Hussain, Development of n-zno/p-si single heterojunction solar cell with and without interfacial layer, PHD thesis, University of North Carolina at Charlotte, 2017 .

[37] R. Sahai and A. G. Milnes, "Heterojunction solar cell calculations", Solid-State Electronics Pergamon Press 1970. Vol. 13, pp. 1289-1299.

[38] S. M. Sze and K. K. Ng, *Physics of semiconductor devices*: John wiley & sons, 2006.

[39] F. Fossard, "Spectroscopie infrarouge de fils et boîtes quantiques d'InAs/InAlAs/InP (001)," Université Paris Sud-Paris XI, 2002.

[40] H. Mathieu and H. Fanet, *Physique des semiconducteurs et des composants électroniques-6ème édition: Cours et exercices corrigés*: Dunod, 2009.

[41] Zeynep Deniz Eygi, Ujjwal Das, Steven Hegedus and Robert Birkmire, "Improved FF in p-si heterojunction solar cells due to optimized ITO/emitter contact", 978-1-4244-9965-6/11/$26.00 ©2011 IEEE.

[42] A. Moliton, *Electronique et optoélectronique organiques*: Springer, 2011.

[43] B. Hussain, "Development of n-ZnO/p-Si single heterojunction solar cell with and without interfacial layer," The University of North Carolina at Charlotte, 2017.

[44] J. Sturm, S. Avasthi, K. Nagamatsu, J. Jhaveri, W. E. McClain, G. Man, A. Kahn, J. Schwartz, and S. Wagner, "Wide bandgap heterojunctions on crystalline silicon," *ECS Transactions,* vol. 58, p. 97, 2013.

[45] J. Zhou, "Indium tin oxide (ITO) deposition, patterning and Schottky contact fabrication," 2006.

[46] R. Chittick, J. Alexander, and H. Sterling, "The preparation and properties of amorphous silicon," *Journal of the Electrochemical Society,* vol. 116, p. 77, 1969.

[47] K. Helali, "Modelisation d'une cellule photovoltaique: etude comparative," Université Mouloud Mammeri, 2012.

[48] A. Labouret and M. Villoz, *Energie solaire photovoltaïque* vol. 4: Dunod, 2006.

[49] A. R. Garfrerick, "Modeling heterogeneous carbon nanotube networks for photovoltaic applications using silvaco atlas software," NAVAL POSTGRADUATE SCHOOL MONTEREY CA2012.

[50] A. Hamrol, F. Górski, D. Grajewski, and P. Zawadzki, "Virtual 3D atlas of a human body–development of an educational medical software application," *Procedia Computer Science,* vol. 25, pp. 302-314, 2013.

[51] D. S. Atlas, "Atlas user's manual," *Silvaco International Software, Santa Clara, CA, USA,* 2005.

[52] I. MALLEM, "Simulation des cellules solaires hétérojonction Si-SiGe par SILVACO," Université Mohamed Khider-Biskra, 2014.

[53] D. Schiavo, "Modeling Radiation Effects on a Triple Junction Solar Cell using Silvaco ATLAS," NAVAL POSTGRADUATE SCHOOL MONTEREY CA2012.

[54] J. C. Fan, F. J. Bachner, and G. H. Foley, "Effect of O2 pressure during deposition on properties of rf-sputtered Sn-doped In2O3 films," *Applied Physics Letters,* vol. 31, pp. 773-775, 1977.

[55]   R. Islam, K. N. Nazif, and K. C. Saraswat, "Si heterojunction solar cells: A simulation study of the design issues," *IEEE Transactions on Electron Devices,* vol. 63, pp. 4788-4795, 2016.

[56]   K. Morigaki, S. Kugler, and K. Shimakawa, *Amorphous Semiconductors: Structural, Optical, and Electronic Properties*: John Wiley & Sons, 2017.

[57]   P. Kumar, P. K. Kanaujia, G. V. Prakash, A. Dewasi, I. Lahiri, and A. Mitra, "Growth of few-and multilayer graphene on different substrates using pulsed nanosecond Q-switched Nd: YAG laser," *Journal of Materials Science,* vol. 52, pp. 12295-12306, 2017.

Abstract

This work is a study by numerical simulation of an of heterojunction solar cells based on conductive oxide/Si heterojunction, the proposed cells are: ITO/Si, ZnO/Si and TiO$_2$ /Si by Silvaco-Atlas software. Using host of improvements, we conclude that there is no big difference between the three studied cells. This does not prevent us from concluding that ZnO(n) /buffer/Si(p) solar cell provides best outputs of the solar cell with: $\eta = 22.30\%$; $J_{sc} = 39.81 mA / cm^2$; $FF = 0.838$; $V_{oc} = 0.668\,V$.

Key words: numerical simulation, Silvaco Atlas, solar cell heterojunction, ZnO, ITO, TiO2, J-V characteristic.

ملخص

هذا العمل عبارة عن محاكاة عددية لخلية شمسية غير متجانسة مكونة من أكسيد موصل/سليكون، الخلايا المقترحة هي:ITO/Si، ZnO/Si ،TiO$_2$ /Si بواسطة برنامج المحاكاة سلفاكو–أطلس وباستخدام مجموعة من التحسينات نجد ان الخلية الشمسيةZnO(n) /buffer/Si(p) لديها أفضل وسائط الخروج المستخرجة من الخاصية جهد–تيار وهي:

$$\eta = 22.30\% \; ; J_{sc} = 39.81 mA / cm^2; FF = 0.838; \; V_{oc} = 0.668\,V.$$

ولكن عموما يوجد تقارب بين وسائط الخروج للخلايا الثلاث.

الكلمات المفتاحية

محاكاة عددية، سلفاكو–أطلس، خلية شمسية غير متجانسة، أكسيد الزنك، أكسيد الانديوم مطعم بالقصدير، أكسيد التيتانيوم، الخاصية تيار–جهد.